REVIEW

Check for updates

Emerging frontiers in chiral metal–organic framework membranes: diverse synthesis techniques and applications

Yun Fan[a] and Mengyun Chen [ID] *[b]

Chirality is a basic and universal property in nature, refering to the asymmetry of molecules, where they do not coincide with their mirror images. Chiral materials, in multiple forms, usually exhibit unique physical phenomena such as chiral luminescence and distinctive chemical properties. Metal–organic framework (MOF) membranes have high porosity and abundant active sites; thus, they are an excellent candidate for functionalization. With the involvement of chiral units, chiral MOF membranes demonstrate great potential in applications such as chiral sensing, separation and luminescence. In this review, we first introduce the up-to-date preparation methods for chiral MOF membranes, including direct and indirect methods, and then discuss their applications in enantiomer recognition, chiral separation, and circularly polarized luminescence. Finally, we summarize the challenges in developing chiral MOF membranes and provide a perspective on future developments.

1. Introduction

Metal–organic frameworks are a type of porous compound formed *via* the self-assembly of metal ions or clusters with organic ligands.[1–3] Owing to their unique properties such as high porosity, large surface area, adjustable pore structure, and accessible active sites, MOFs have broad applications in separation, catalysis, sensing, and energy storage.[4,5] Research on MOF materials is gradually shifting from bulk materials to membrane materials, as membranes offer advantages such as low cost, low energy consumption and reusability, which are important for their practical applications.[6–8]

Chiral molecules are interesting materials and exhibit unique physical phenomena, such as chiral luminescence and distinctive chemical properties. Chiral materials share similar structures but can possibly present completely different physicochemical or biological properties.[9,10] For example, one enantiomer performs the desired function, while the other shows an inactive state or, in some cases, even causes unwanted side effects, which are significant in drug and food safety as well as chemical synthesis.[11,12]

Owing to the abundant active sites of MOFs, chiral MOFs have been successfully fabricated by incorporating chiral units *via* various methods (*e.g.* addition of chiral ligands or chiral secondary structural units, post modification, or chiral induction).[13–16] Based on chiral MOF materials, researchers have developed chiral MOF membranes for practical applications.[17] With an ordered pore structure resulting from the arrangement of crystal growth, chiral MOF membranes provide better recognition and separation of enantiomers, *e.g.* chiral drugs and chiral gas molecules.[18–20] By integrating fluorescent units, chiral MOF membranes present circularly polarized luminescence (CPL), which has potential for applications in information storage, anti-counterfeiting, and encryption.[21] In summary, chiral MOF membranes, as emerging functional materials, have seen great progress in preparation and applications, which inspired us to provide a summary.

In this review, we first introduce the preparation of chiral MOF membranes, including direct methods (solvothermal synthesis, layer-by-layer (lbl) synthesis, and template-assisted synthesis) and indirect methods (solution casting and thermally induced phase separation-hot pressing (TIPS-HoP)) (Fig. 1).[22–24] Then, we summarize the applications of chiral MOF membranes in chiral sensing, chiral separation, and CPL. Finally, we provide insights into the preparation of high-quality chiral MOF membranes for enhanced applications.
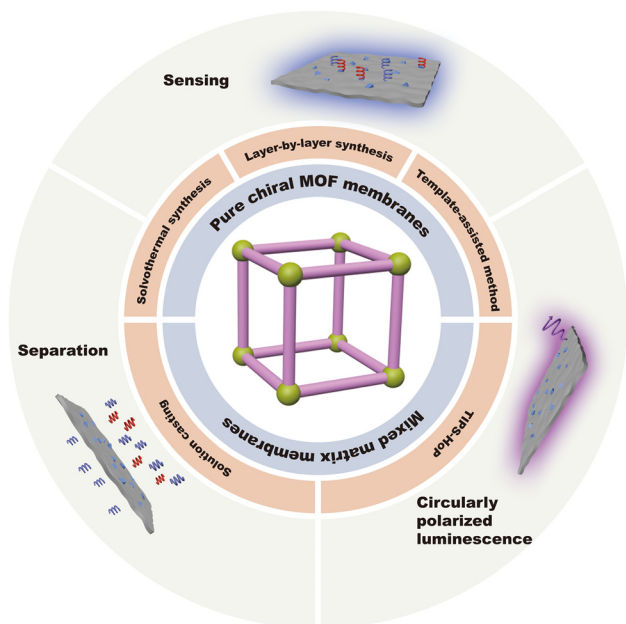
2. Preparation of chiral MOF membranes

There are two main forms of chiral MOF membranes—pure membranes and mixed matrix membranes (MMMs)—based on the presence of a matrix. Direct methods are typically used

*a*Key Laboratory of Flexible Electronics (KLOFE), Institute of Advanced Materials (IAM) & School of Flexible Electronics (Future Technologies), Nanjing Tech University, 30 South Puzhu Road, Nanjing 211816, China
*b*Department of Physics, Chemistry and Biology (IFM), Linköping University, Linköping, 58183 Sweden. E-mail: mengyun.chen@liu.se

Fig. 1 Summary of the preparation strategies and applications of chiral MOF membranes.

for the synthesis of pure chiral MOF membranes, while indirect methods are used for the synthesis of MMMs. The synthesis of pure chiral MOF membranes is simple and usually involves a one-step process on the substrate. Self-supporting MMMs are prepared by synthesizing chiral MOF materials followed by membrane fabrication. Due to their combination with various matrices, chiral MOF MMMs offer the advantages of enhanced mechanical stability and processability, which ensures a simultaneous increase in permeability and selectivity.[25] The methods for preparing pure chiral MOF membranes and MMMs are discussed in the following section.

2.1. Pure chiral MOF membranes

Pure chiral MOF membranes are synthesized from chiral MOF precursors *via in situ* synthesis on substrates, including one-pot solvothermal, lbl, and template-assisted synthesis.

2.1.1. One-pot solvothermal synthesis. In this method, substrates are immersed in a chiral precursor solution, allowing chiral MOF membranes to grow directly on them. This approach is simple and efficient, and it ensures high thermal stability of membranes. Anodic aluminum oxide (AAO) substrates are frequently used in the preparation of chiral MOF membranes. For example, Wang *et al.* reported the preparation of L-His-ZIF-8 membranes with good continuity through an *in situ* growth method.[19] The L-His-ZIF-8 membrane was prepared by placing the AAO substrate horizontally in a precursor solution containing Zn ions, 2-methylimidazole (Hmim), and L-histidine (L-His), which completely covered the AAO substrate and resulted in high integrity. The characteristic peaks of amino and carboxylic groups observed in the membrane indicated that L-His, as the ligand molecule, was successfully incor-
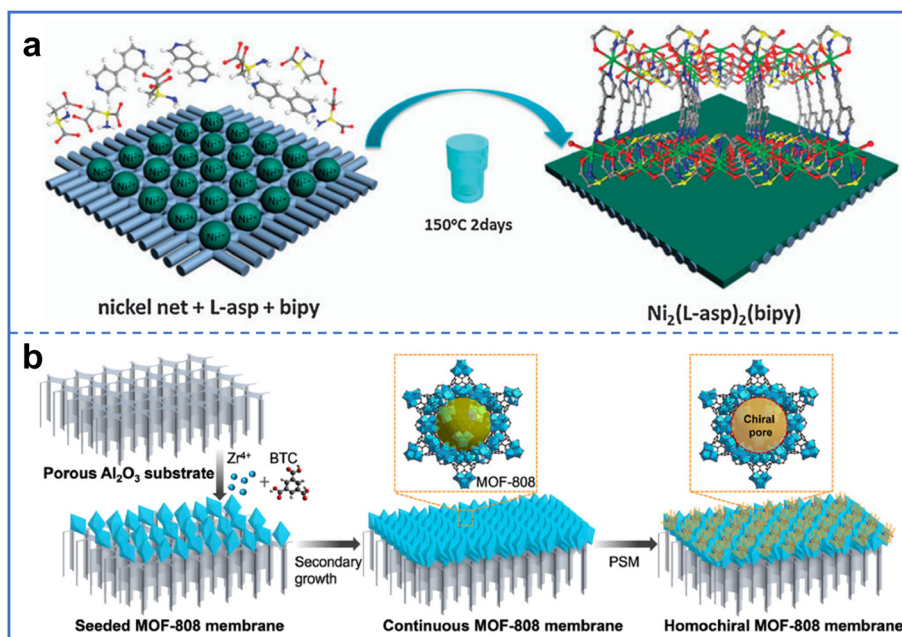
porated into the ZIF-8 framework, endowing the MOF with chirality and providing a chiral channel for the separation of enantiomers.

In addition, metal source substrates are usually used to prepare MOF membranes, which not only serve as substrates but also participate in the synthesis.[26] Qiu *et al.* prepared a $Ni_2(L\text{-asp})_2(bipy)$ membrane on a Ni net substrate using a solvothermal method with a thickness of 10–20 μm (Fig. 2a).[27] The Ni net was horizontally placed in the autoclave and reacted with a solution of 4,4′-bipyridine (bipy) and L-aspartic acid (L-asp) ligands. The Ni ions in the Ni net acted as anchoring active sites, coordinating with organic ligands to promote the nucleation and growth of MOFs. $Ni_2(L\text{-asp})_2(bipy)$ grew around the wires of the Ni net and then alternately grew to form a continuous $Ni_2(L\text{-asp})_2(bipy)$ membrane, creating strong adhesion between the membrane and the Ni net substrate. A thin and defect-free $Ni_2(L\text{-asp})_2(bipy)$ membrane was prepared using this single metal source method because the formation of a layer of the membrane led to the cessation of the growth process due to the absence of a metal source. X-ray diffraction and scanning electron microscopy (SEM) characterization indicated the high crystallinity and continuity of the $Ni_2(L\text{-asp})_2(bipy)$ membrane.

In situ secondary growth of MOFs on substrates was used to obtain continuous and well-intergrown MOF membranes. Recently, Zhao *et al.* synthesized chiral MOF-808 membranes on α-aluminum oxide (α-Al_2O_3) substrate through secondary growth and post-synthetic modification (Fig. 2b).[23] First, the α-Al_2O_3 substrate was vertically placed in the precursor solution of MOF-808 for a solvothermal reaction to prepare a seeded MOF-808 membrane. The membrane was then placed in a precursor solution of MOF-808 for secondary growth to obtain a continuous MOF-808 membrane. Subsequently, the chiral MOF-808 membranes MOF-808-Ala, MOF-808-Thr, and MOF-808-His were grown after reacting in solutions containing the chiral molecules L-alanine (L-Ala), L-threonine (L-Thr), and L-His, respectively. The introduced amino acid molecules partially replaced the trifluoroacetic acid regulator on the Zr cluster to coordinate with the unoccupied Zr cluster, thus being integrated into the MOF-808 structure. The chiral MOF-808 membranes obtained by post-synthetic modification retained the crystallinity of MOF-808, and their thicknesses could be controlled by regulating the concentration of metal ions.

2.1.2. Layer-by-layer synthesis. In this method, chiral MOF materials are deposited on the substrate layer by layer, forming chiral MOF membranes with controllable thickness and low surface roughness. Heinke *et al.* prepared a nanoporous chiral pillared-layer $Cu_2(DCam)_2(AzoBiPyB)$ (DCam was D-camphoric acid, AzoBiPyB was (E)-2-(phenyldiazenyl)-1,4-bis(4-pyridyl) benzene) membrane on the substrate using the controlled lbl method.[28] The pillar ligand AzoBiPyB in the chiral MOF provided photoswitchable property, while the interlayer ligand DCam provided chirality. First, the substrate was immersed in a metal salt solution for 15 min, washed with ethanol and immersed in the mixed ligand solution for 30 min. After

Fig. 2 (a) Preparation of thin chiral $Ni_2(L-asp)_2(bipy)$ membrane with Ni net asboth substrate and metal source. Reproduced with permission from ref. 27. Copyright 2013, The Royal Society of Chemistry. (b) Preparation of chiral MOF–808 membranes by introduction of chiral molecules to MOF–808 membranes. Reproduced with permission from ref. 23. Copyright 2024, American Chemical Society.

washing with ethanol, the above process was repeated, and a thin surface-mounted MOF membrane was grown layer by layer by alternately exposing the substrate to the precursor solutions. The thickness of the MOF membrane could be controlled by changing the number of immersion cycles in the precursor solutions. The preparation of chiral MOF membranes on substrates in aqueous solution can be achieved by selecting appropriate self-assembled monolayers (SAM) to modify the substrate. Gu *et al.* selected octathiolated γ-cyclodextrin $(\gamma CD(SH)_8)$ as the SAM to modify the Au substrate to prepare highly oriented surface-coordinated MOF $(\gamma CD$-SURMOF) membranes (Fig. 3a).[29] The $\gamma CD(SH)_8$ with eight thiol groups reacted with Au to form thiolate bonds and was anchored on the Au surface, achieving surface functionalization of the Au substrate. The modified Au substrate $(Au(\gamma CDS_8))$ was then immersed in K ions and γCD aqueous solutions, and the γCD-SURMOF was prepared by repeated lbl assembly. Unlike the chiral MOF membranes prepared from ethanol solution, the modified Au substrate did not require washing after each immersion step. The thickness of γCD-SURMOF could be controlled by the number of immersion cycles, and the membrane thickness increased with increasing number of immersion cycles. Because $Au(\gamma CDS_8)$ induced direct nucleation, where the γCD ring is oriented parallel to the substrate in the presence of thiolate anchoring groups, the γCD-SURMOF exhibits a [110] orientation perpendicular to the substrate.
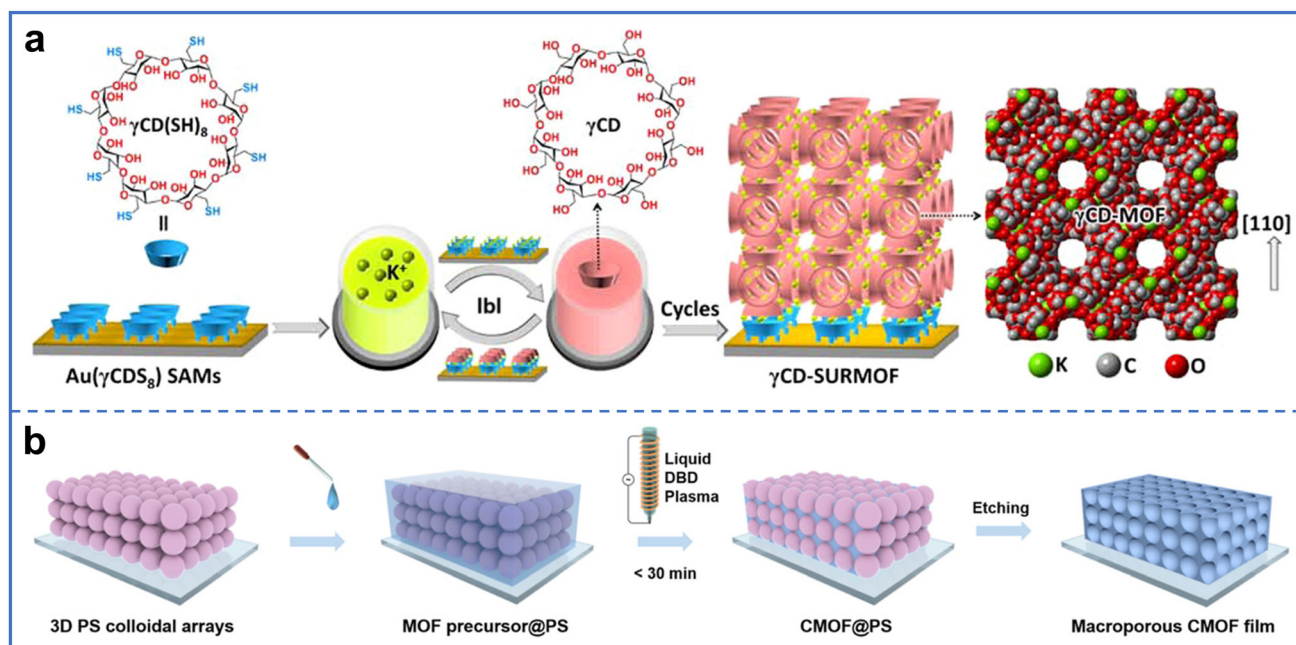
2.1.3. Template-assisted method. In this method, templates are used to provide extra pore structures for MOF membranes. Cui *et al.* recently reported the preparation of chiral His-ZIF-8,

$[Cd(LTP)_2]_n$, and $[Cu(mal)bpy]·H_2O$ membranes using a template-assisted method, which not only possessed the inherent micropores in MOFs but also ordered macropores derived from the template (Fig. 3b).[30] Polystyrene spheres (PSs) were assembled on a glass slide to form highly ordered three-dimensional (3D) PS colloidal arrays, which were used as templates for MOF growth. The PS arrays were then immersed into the precursor solution of the chiral MOFs and introduced into the liquid dielectric barrier discharge (DBD) plasma reactor. Three different chiral MOFs were grown in the interstices of PSs using the DBD plasma induction method. The PS template was then removed by etching to obtain macro–microporous chiral MOF (M-CMOF) membranes with hierarchical porous structures of macropores and micropores. The preparation of chiral MOFs by liquid DBD plasma-induced crystallization is a green synthesis approach with the advantages of short synthesis time, low cost, and low energy consumption. The three M-CMOF membranes exhibited good crystallization before and after template removal, with the macropores of approximately 200 nm. The M-L-His-ZIF-8 membrane exhibited an ultrathin thickness of ~3.9 μm. The presence of the C=O stretch of the chiral molecule L-His and the disappearance of N–H vibration indicated that the chiral molecule was incorporated into the MOF framework.

2.2. Chiral MOF MMMs

Chiral MOF MMMs are hybrid membranes in which chiral MOF fillers are embedded in a continuous matrix.[31] The chiral MOF MMMs exhibit higher mechanical strength, fewer defects, and better continuity due to the combination of the

Fig. 3 (a) Preparation of γCD-SURMOF membrane by assembly of metal ions and ligands layer by layer onto γCD(SH)$_8$ modified Au substrates. Reproduced with permission from ref. 29. Copyright 2022, Chinese Chemical Society. (b) Preparation of M-CMOF membranes with hierarchical porous structures by using PS arrays as templates. Reproduced with permission from ref. 30. Copyright 2024, American Chemical Society.

matrix. The synthesis of chiral MOF materials and the preparation of MMMs are described in the following sections.
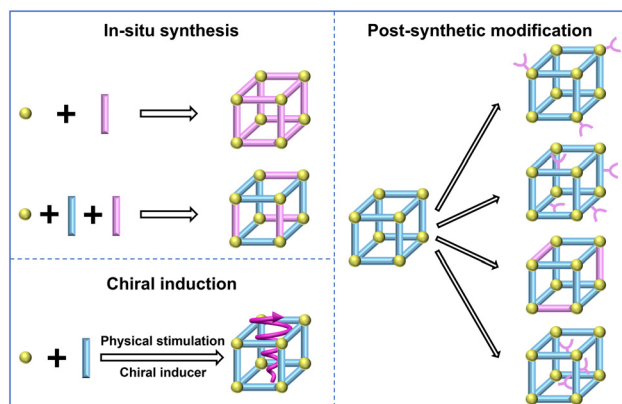
2.2.1. Preparation of chiral MOFs. The quality of chiral MOF materials significantly affects the properties of chiral MOF MMMs. There are three main methods: *in situ* synthesis, post-synthetic modification, and chiral induction, which are suitable for synthesizing various chiral MOFs (Fig. 4).[32,33]

In situ synthesis. The *in situ* synthesis is the most widely used method for synthesizing chiral MOFs, and the synthesized chiral MOFs exhibit bulk uniformity and high enantiomeric
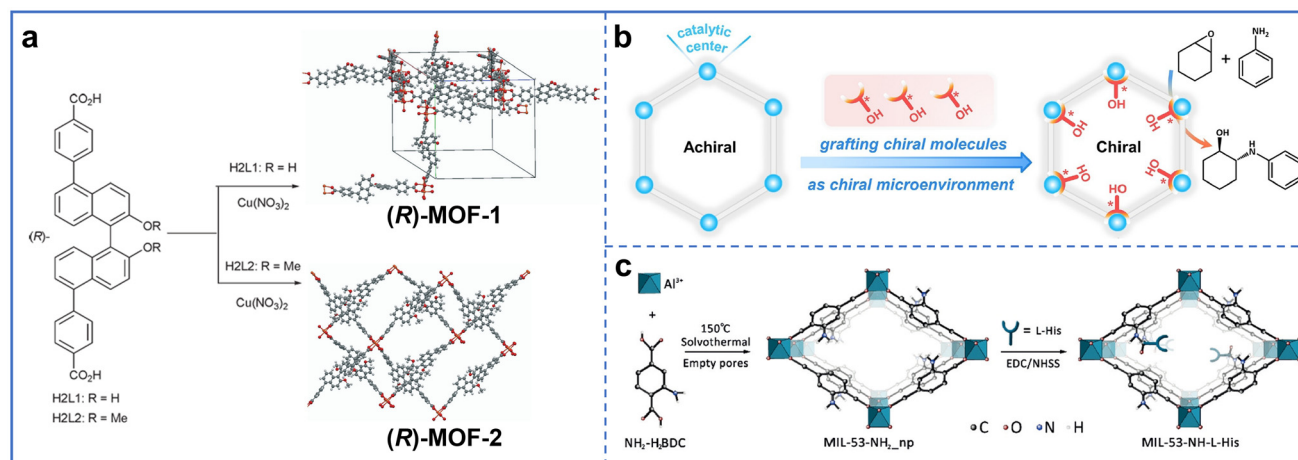

Fig. 4 Preparation methods for chiral MOFs include *in situ* synthesis, post-synthetic modification, and chiral induction. Yellow balls represent metal nodes, blue sticks represent organic ligands, purple sticks represent chiral ligands, and purple Y-shaped curves represent chiral molecules.

purity.[34–36] The method involves enantiomeric chiral ligands, which are expensive, causing complexity and high cost in the synthesis.

Tanaka *et al.* synthesized chiral ligands (*R*)-2,2′-dihydroxy-1,1′-binaphthyl-5,5′-dibenzoic acid (H$_2$L1) and (*R*)-2,2′-dimethoxy-1,1′-binaphthyl-5,5′-dibenzoic acid (H$_2$L2) for chiral interpenetrating (*R*)-MOF-1 and non-interpenetrating (*R*)-MOF-2, respectively (Fig. 5a).[37] In (*R*)-MOF-1, Cu ions coordinated with the four oxygen atoms in the carboxylic acid group of H$_2$L1 to form layers in the topological structure. Then, each two-dimensional (2D) network was interpenetrated in a parallel or parallel tilted manner to form (*R*)-MOF-1. The 2D network structure in (*R*)-MOF-2 was like that in (*R*)-MOF-1, but the 2D network did not interpenetrate but overlapped to form (*R*)-MOF-2. In addition, Wang *et al.* synthesized homochiral ʟ-His-ZIF-8 using mixed ligands.[19] The chiral molecule ʟ-His was introduced into the precursor solution of ZIF-8, and then ʟ-His-ZIF-8 was formed by the solvothermal self-assembly of ʟ-His with Hmim and Zn ions.

The *in situ* synthesis method has also been used to synthesize chiral MOF nanosheets with highly ordered in-plane nanopores, which exhibit excellent performance in catalysis, sensing, and separation. For example, Cui *et al.* synthesized chiral layered Eu-MOFs using dicarboxylic acids derived from 1,1′-biphenyl phosphoric acid as chiral ligands.[38] The Eu ions were coordinated with four bidentate bridges and four chelating carboxylate groups in the six ligands. Two adjacent Eu ions were connected by four carboxylate groups to form a planar framework, which was then stacked vertically to form the layered structure. The layered Eu-MOF was exfoliated into

Fig. 5 (a) Preparation of chiral (*R*)-MOF-1 and (*R*)-MOF-2 with chiral molecules H₂L1 and H₂L2 as ligands through *in situ* synthesis. Reproduced with permission from ref. 37. Copyright 2015, The Royal Society of Chemistry. (b) Preparation of chiral (*R*)-C$_n$@PCN-222(Cu) by anchoring chiral molecules onto Zr clusters in PCN-222(Cu). Reproduced with permission from ref. 43. Copyright 2023, Wiley-VCH. (c) Preparation of chiral MIL-53-NH-L-His by grafting L-His onto the ligands of MIL-53-NH₂(Al). Reproduced with permission from ref. 44. Copyright 2019, Wiley-VCH.

chiral MOF nanosheets (1-MONs) using solvent-assisted liquid sonication due to weak interlayer interactions between the layers.

Post-synthetic modification. This method involves introducing chiral molecules into the as-synthesized achiral MOFs to endow them with chiral characteristics without altering their topological structure.[39–42] When there are active sites in MOFs, chiral molecules can be grafted onto the metal clusters or organic ligands of MOFs through coordination or covalent interactions. This method has been successfully applied to a wide range of chiral MOFs, as it starts from achiral materials, with the chirality introduced in a separate process. However, compatibility and interaction between the chiral molecules and the MOF framework must be carefully considered during the selection of chiral molecules.

PCN-222(Cu) is an achiral MOF formed by the coordination of Zr ions, [5,10,15,20-tetrakis(4-carboxyphenyl) porphyrinato]-Cu(II) (Cu-TCPP), and benzoic acid (Fig. 5b).[43] By anchoring chiral hydroxylated molecules with different carbon chain lengths onto unsaturated coordination sites of Zr clusters, a series of (*R*)-C$_n$@PCN-222(Cu) (*n* = 1, 2, 3) was obtained. There were approximately 3.8–3.9 chiral molecules grafted onto each Zr cluster on average, indicating that chiral molecules completely replaced the –OH groups on the Zr clusters and co-ordinated with the Zr clusters.

Wang *et al.* introduced the chiral molecule L-His, which coordinates with the functional groups of ligands, to convert achiral MIL-53-NH₂(Al) into chiral MIL-53-NH-L-His (Fig. 5c).[44] The achiral MIL-53-NH₂(Al) was formed by the coordination assembly of Al clusters with 2-aminoterephthalic acid (NH₂BDC) with a flexible framework structure, which was conducive to immobilizing guest molecules. The carboxylic group in L-His underwent an amidation reaction with the amino group in NH₂BDC to graft L-His into the MOF framework, endowing MIL-53-NH₂(Al) with chirality.

In addition to grafting chiral molecules onto ligands, chiral MOFs can be formed by replacing achiral ligands in MOFs. Cui *et al.* used a solvent-assisted ligand exchange strategy to incorporate chiral ligand linear dicarboxylate linkers (H₂L^M) into UiO-68-Me.[45] The H₂L^M molecule had a similar length and connectivity with the ligand (2-methyl-terphenyl dicarboxylate ligand) H₂TPDC-Me in UiO-68-Me.

Incorporating chiral guests into the pores of MOFs is also a post-synthetic modification method. The chiral molecules [Rh (Me-BPE)(cod)]OTf (Me-BPE = 1,2-bis(2,5-dimethyl-phospholano)ethane, cod = 1,5-cyclooctadiene, OTf = triflate) were encapsulated into the pores of UMCM-1-NH₂, endowing the MOF with chiral properties, which exhibited excellent enantioselectivity in the asymmetric hydrogenation reactions of unsaturated olefins.[46] During the post-synthetic modification process, it is necessary to strictly control the reaction conditions to avoid damaging the MOF framework structure.

Chiral induction. Chiral induction is based on achiral precursors, where the symmetry breaking and induction of chiral arrangement in building units are caused by physical stimulation such as CPL irradiation or adding inducing agents.[47–49] The chiral induction method is relatively simpler and less expensive but gives less pure products.

Wu *et al.* synthesized the coordination polymer [{*P/M*-Cu (succinate)(4,4′-bipyridine)}$_n$]·(4H₂O)$_n$ using CPL irradiation.[50] According to the analysis of CPL chirality and the corresponding obtained products, the product after left-handed CPL irradiation showed a left-handed helical structure, whereas right-handed CPL irradiation was beneficial for the production of right-handed helical structure crystals. The Cu ions co-ordinated with succinic acid to form an intermediate fragment [Cu(succinate)]$_x$ that exhibited helicity. CPL irradiation stimulated the conversion of fragment [Cu(succinate)]$_x$ into the preferential configuration, which then assembled into a 3D structure with chirality by coordination with 4,4′-bipyridine.

In addition to physical stimulation, the introduction of chemical reagents can induce chirality by affecting the self-assembly of MOFs. Enantiomeric pure organic acids D-(+)-camphoric acid (D-(+)-H$_2$cam) and L-(−)-camphoric acid (L-(−)-H$_2$cam) were used to induce the asymmetric crystallization of achiral manganese damantane-1,3-dicarboxylic ([Mn(adc)]) (Fig. 6a).[51] When using D-(+)-H$_2$cam as a chiral inducer, the main product was (+)-[Mn$_3$(HCOO)$_4$(adc)]; when L-(−)-H$_2$cam was used as a chiral inducer, the main product was (−)-[Mn$_3$(HCOO)$_4$(adc)]. The synergistic effect of chiral H$_2$cam and achiral H$_2$adc led to the asymmetric crystallization of the product. H$_2$cam coordinated with Mn clusters to control the absolute helicity of the [Mn$_3$(HCOO)$_4$]$_n^{2n+}$ framework. The H$_2$cam in the crystal was then replaced by H$_2$adc ligands to form chiral MOFs, and H$_2$cam was not incorporated into the MOF structure. Hong et al. introduced chiral intermediates I(M) or I(P) to the assembly with achiral pyridine, ligand benzene-1,3,5-tris(4-benzoic acid) (H$_3$BTB) and Zn ions to prepare chiral FJI-H27(M) and FJI-H27(P) (Fig. 6b).[52] Pyridine, as a template, participated in the coordination-driven assembly, the amount of which provided the precise regulation of the chirality.

In conclusion, in situ synthesis offers high enantiomer purity and stability, even though it is complex and expensive and usually requires high temperatures and pressures. Post-synthetic modification is a general method in which the compatibility of the introduced chiral molecules and MOFs is required. The chiral induction method is simple and cost-effective, even though the chiral purity achieved is modest. Depending on the requirements of chiral MOFs, various preparation methods are available.
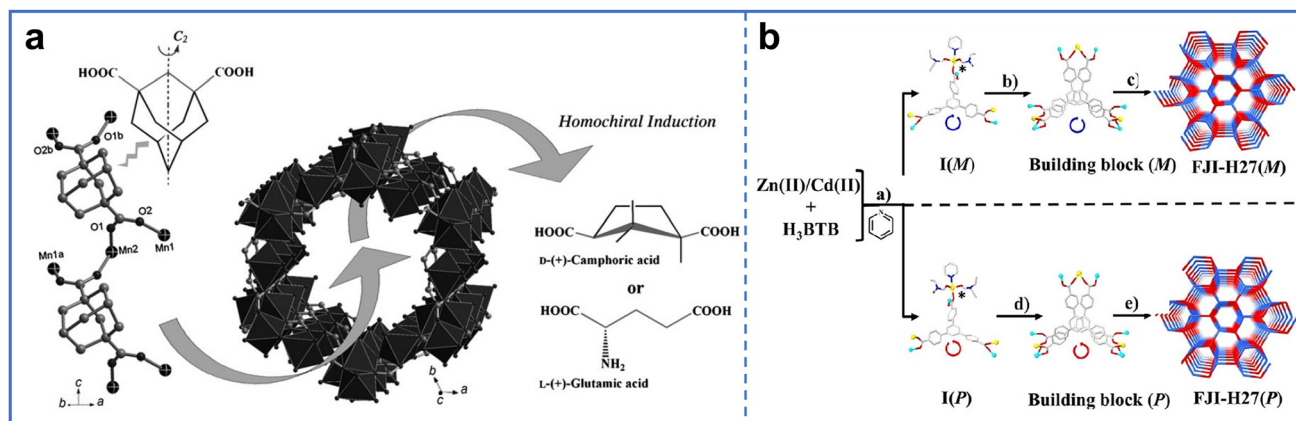
2.2.2. Preparation of chiral MOF MMMs. Chiral MOF MMMs are prepared by dispersing chiral MOF particles in a matrix and using specific molding processes to obtain membranes with chiral properties. The key to this preparation approach is the uniform dispersion and good interfacial compatibility of MOF particles with the matrix. Polymers are widely used as a matrix for chiral MOF MMMs because polymers are soft and provide functional groups to interact with the ligands of MOFs. The preparation methods of chiral MOF MMMs include solution casting and TIPS-HoP.
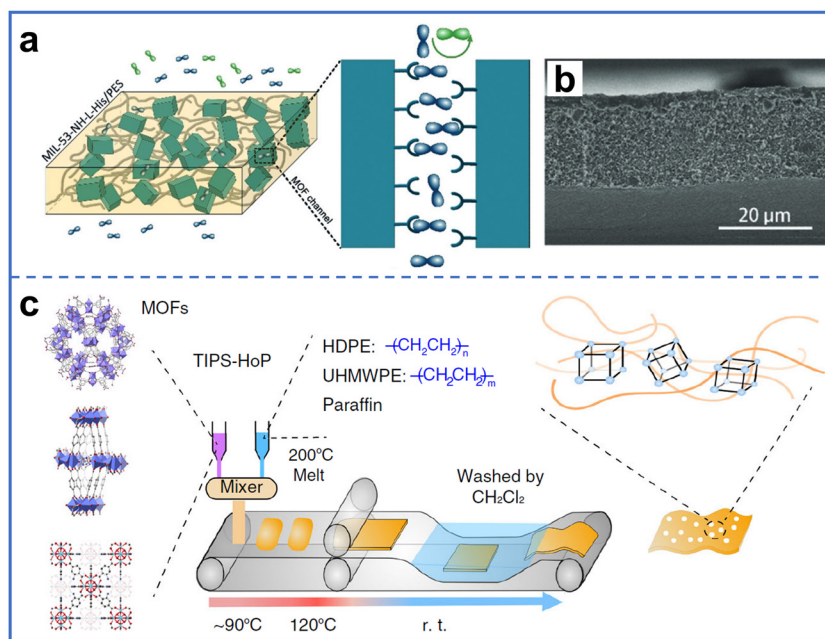
Solution casting. The solution casting method involves mixing chiral MOFs with polymers and casting them into a membrane, followed by appropriate post-treatment to obtain the final MMMs, which is simple and suitable for large-scale production. Wang et al. prepared MIL-53-NH-L-His-based MMMs by depositing the membrane onto a substrate using a casting blade to apply solution or paste (Fig. 7a).[44] First, a small amount of polymer polyethersulfone (PES) was added to chiral MOF particle dispersions to reduce the aggregation of MOF particles in the polymer. Then, the remaining PES was added to the dispersion, and the mixture was stirred evenly. Subsequently, the mixture was dropped onto a glass substrate and spread onto a membrane on the substrate using a casting blade. As the solvent evaporated, MIL-53-NH-L-His-based MMM was formed, which could be peeled off from the glass substrate after cooling to obtain a self-supporting membrane. MIL-53-NH-L-His particles were uniformly distributed in the membrane without cracks and defects (Fig. 7b). The loading of MOFs in the membrane could be regulated by changing the ratio of added MOFs. MMMs with different loading ratios of MOFs retained the crystal structure of the MOF particles, indicating that the manufacturing process of the membrane did not affect the crystal structure of the MOFs.

Subsequently, the group used the same preparation method to mix chiral MOF γ-CD-MOF with PES to prepare CD-MOF/PES MMMs.[53] In addition to PES as the polymer substrate, poly(vinylidene fluoride) (PVDF) was also employed as the dispersed matrix for yolk-shell L-His&R6G@ZIF-8 particles in the preparation of MMMs.[54] The casting blade technology is simple and effective for preparing MMMs with controlled thickness and surface roughness.

TIPS-HoP. This method involves roll-to-roll hot pressing of a mixture of ultra-high molecular weight polymer interwoven

Fig. 6 (a) Preparation of chiral [Mn$_3$(HCOO)$_4$(adc)] by chiral induction with H$_2$cam. Reproduced with permission from ref. 51. Copyright 2010, Wiley-VCH. (b) Preparation of chiral FJI-H27(M) and FJI-H27(P) chiral induction with pyridine. Reproduced with permission from ref. 52. Copyright 2021, Wiley-VCH.

Fig. 7 (a) Preparation of self-supporting MMMs by solution casting method with chiral MIL–53–NH–L–His dispersed in PES. (b) SEM image of the cross-section of MMMs with 20 wt% MIL–53–NH–L–His loading. Reproduced with permission from ref. 44. Copyright 2019, Wiley-VCH. (c) Prrparation of MMMs with high MOF loading by chiral Zn-BLD dispersed inmixed HDPE and UHMWPE polymers through TIPS-HoP method. Reproduced with permission from ref. 55. Copyright 2019, Springer Nature.

MOF particles onto a belt to form MMMs, which usually help achieve membranes with good flexibility and ultrahigh MOF loading. MOFs act as molecular sieving channels in MMMs, in which the separation performance can be effectively improved by increasing the loading of MOFs.

Wang *et al.* prepared MMMs using the TIPS-HoP approach, which overcame the challenge of loss of mechanical strength in high MOF-loading membranes (Fig. 7c).[55] First, chiral Zn-BLD was added to the paraffin, high-density polyethylene (HDPE), and ultrahigh-molecular-weight polyethylene (UHMWPE) mixed melt, and it was continuously stirred to disperse evenly. UHMWPE was introduced into the membrane to connect MOF particles, ensuring the flexibility of the membrane under ultrahigh MOF loading. Paraffin was used as the flowable agent to reduce the melt viscosity of HDPE and UHMWPE, thereby avoiding the formation of membranes with brittleness and impermeability. Then, the mixture was dropped onto a belt and transferred to the middle of two rollers for roll-to-roll hot pressing to form the MMM. Finally, the Zn-BLD PE MMM was formed by soaking the membrane in dichloromethane to remove the paraffin from the membrane. In addition to chiral Zn-BLD, achiral MOFs such as NH$_2$-UiO-66, MIL-100(Cr), MOF-5, and ZIF-8 could be prepared as MMMs using this approach, demonstrating the universality of this strategy. Typically, the mechanical properties of MMMs decrease with the increase in MOF loading.[56,57] However, the MMM with 86% MOF (Zn-BLD PE MMM-86%) loading maintained flexibility without forming cracks after bending. MOF particle aggregates and long-chain polymers interwove in Zn-
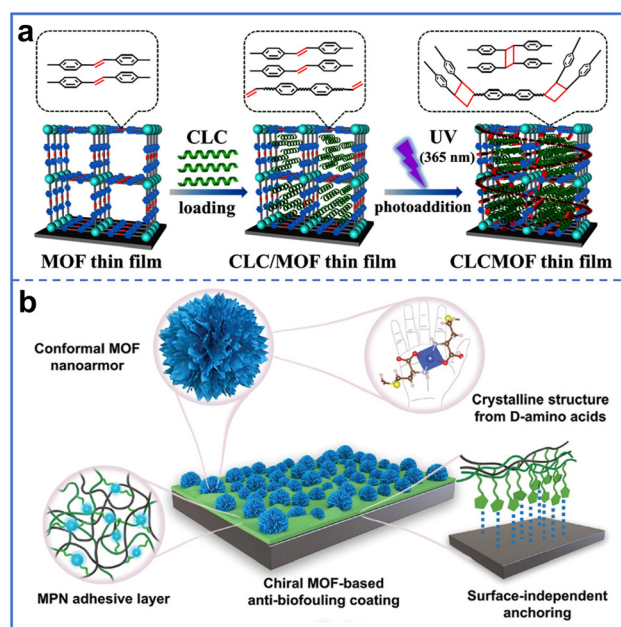
BLD PE MMM-86%, forming hierarchical porous structured MMM with the inherent micropores of MOFs and the macropores originating from the interweaving of MOF particles.

Recently, some reports have investigated new matrices for chiral MOF MMMs. A chiral liquid crystal (CLC) was introduced to combine with MOFs to prepare a CLC MOF (CLCMOF) membrane. Gu *et al.* prepared a CLCMOF membrane by combining CLC with Zn$_2$(sdc)$_2$ (Fig. 8a).[58] The CLC solution was a mixture of *R*-obob, 2-methyl-1,4-phenylene bis(4-(3-(acryloyloxy)propoxy) benzoate), and 4-[[6-[(1-oxo-2-propen-1-yl)oxy]hexyl]oxy]-,4-methoxyphenyl ester in a certain proportion, which encapsulated into the pores of Zn$_2$(sdc)$_2$ due to cross-linking reaction between alkenyl groups in CLC and stilbene groups in MOF ligands under ultraviolet light (UV) irradiation. The CLCMOF membrane exhibits LC thermotropic properties and excellent transparency. The crystal structure of Zn$_2$(sdc)$_2$ was not destroyed by the cross-linking reaction with CLC, allowing the CLCMOF membrane to retain the crystallinity of the MOFs.

Xu *et al.* used an amorphous metal-polyphenol network (MPN) as the matrix for an amorphous/crystalline heterogeneous structure chiral MOF membrane (MPN-DMOF) (Fig. 8b).[59] MPN was prepared by a mixed solution of Cu^{2+}, polyethylenimine, and tannic acid, and provided abundant nucleation sites, where the D-methionine chelated with Cu ions to form MOFs. The MPN-DMOF coating retained the crystal structure and phase purity of D-Met@MOF, which was constructed by Cu clusters with D-methionine ligands.

Pure chiral MOF membranes provide high porosity and more accessible active sites despite their high cost and lack of

Fig. 8 (a) Preparation of CLCMOF membrane by encapsulateion of CLC into the pores of achiral MOFs. Reproduced with permission from ref. 58. Copyright 2024, American Chemical Society. (b) Preparation of chiral MOF membrane (MPN-DMOF) by reaction of chiral ligands with MPN matrix. Reproduced with permission from ref. 59. Copyright 2024, Wiley-VCH.

self-supporting possibility. Chiral MOF MMMs have excellent mechanical strength and more convenient applications as self-supporting membranes. However, the interface compatibility between MOFs and matrices, as well as the aggregation of MOF particles, still requires improvement for high-quality MMMs.

3. Applications of chiral MOF membranes

The high porosity and high density of reactive sites ensure that chiral MOF membranes have great potential for chiral recognition and enantiomer separation.[60–62] By the involvement of luminescent units in various ways, chiral MOF membranes also present excellent CPL properties, which make them potential for applications in optical display and information storage fields.[63] We discuss the applications of chiral MOF membranes in sensing, separation, and CPL in the following section.

3.1. Sensing

Due to the abundant active sites and decoration of chiral units, chiral MOF membranes interact differently with chiral enantiomers, and they have been successfully applied as sensors to distinguish chiral isomers.[64–67]

Cui *et al.* dispersed chiral 1-MONs into PES to prepare self-supporting MMM (1-MONs-MMM) for detecting terpenes and
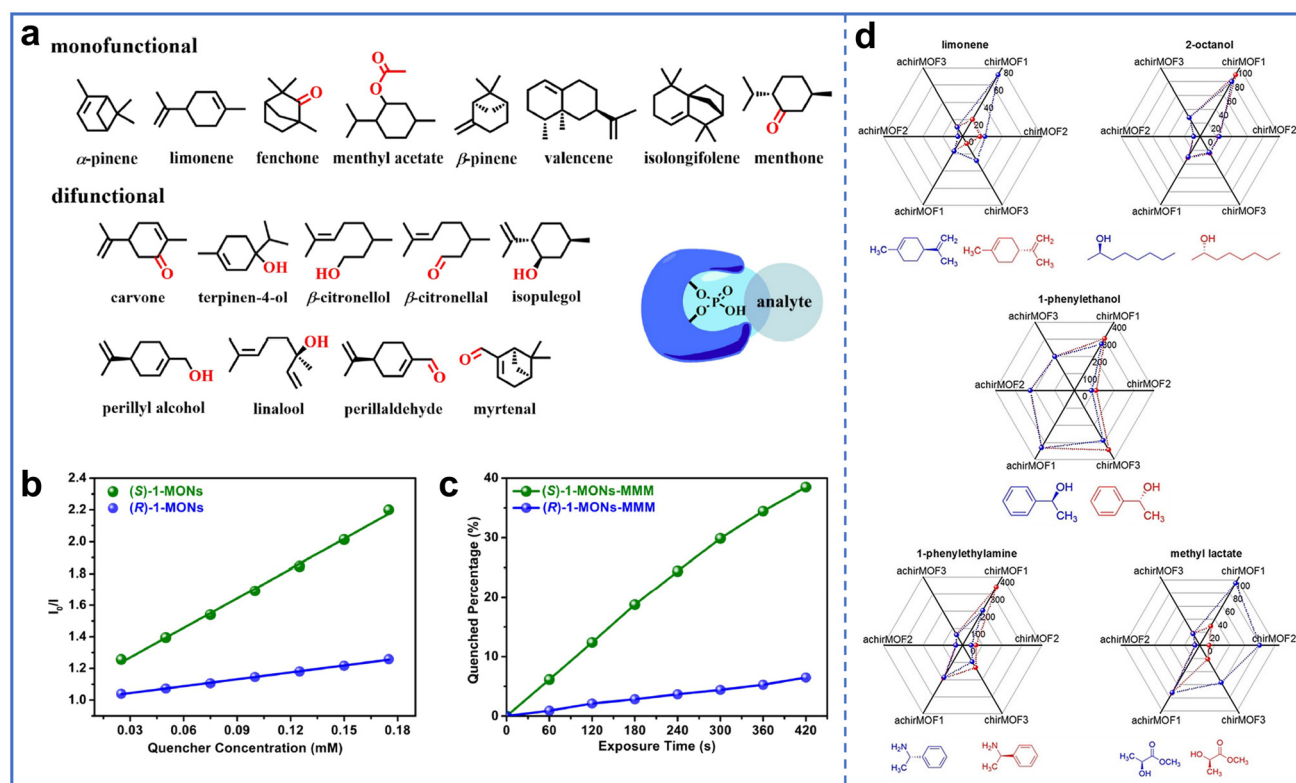
terpenoids, which was a challenging enantiomer detection issue.[38] 1-MONs-MMM exhibited an emission peak at 355 nm, which was blue shifted compared to 386 nm of 1-MONs in acetonitrile solvent. This may be due to the influence of the PES matrix in the MMM on the fluorescence emission. The phosphoric acid active sites in 1-MONs interacted with the double bonds or carbonyl groups in terpenes and terpenoids, which induced changes in the structure of the nanosheets, such as conformational and exciton binding changes or hardening, leading to fluorescence quenching and selective recognition of enantiomers (Fig. 9a). When MMMs were exposed to (−)-linalool vapor, the fluorescence of (*S*)-1-MONs-MMM and (*R*)-1-MONs-MMM was quenched (Fig. 9b). After 420 s, the quenching percentage of (*S*)-1-MONs-MMM reached 38.5%, whereas the quenching percentage of (*R*)-1-MONs-MMM could only reach 6.5%, corresponding to the enantioselectivity factor of 9.03 (Fig. 9c). MMMs selectively recognized not only chiral vapors with single functional groups such as α-pinene, limonene, and fenchone, but also terpenoids with chiral bifunctional groups, including terpinen-4-ol and β-citronellol. In addition to chiral MOF nanosheets, L-His&R6G@ZIF-8 with a unique yolk-shell structure, MMMs have been prepared as optical sensors for highly sensitive and selective detection of L-proline.[54]

To simultaneously identify multiple molecules and their enantiomers, a sensor array comprising different sensors for identifying enantiomers was proposed.[68] Heinke *et al.* prepared an enantioselective electronic nose (e-nose) based on a chiral MOF sensor array and used for the detection of chiral odor molecules through machine learning.[69] Three chiral MOFs and three achiral MOFs were prepared as quartz-crystal microbalance (QCM) sensors, which were integrated into the sensor array. In the e-nose, achiral MOFs were only used to distinguish different molecules that exhibited the same response as chiral isomers, while chiral MOFs were used to recognize enantiomers. When the sensor array was exposed to odor molecules, the contact between the MOF membranes and the odor molecules caused a frequency shift in resonance frequency to achieve a response to the odor molecules, and the sensor response was linearly correlated with the concentration of the odor molecules. The sensor array exhibited selective recognition of ten isomers with an average accuracy of 96.1%, achieving high selectivity recognition (Fig. 9d).

Subsequently, the same group used MOF membrane sensor arrays to detect mixtures of ternary xylene isomers.[70] The accuracy of e-nose in distinguishing isomers of xylene mixtures with concentrations of 10 and 100 ppm was evaluated. Using machine learning algorithms to analyze the sensor array data, the composition of the mixture was determined. The accuracy of the mixture with a 10 ppm concentration was 86%, and the accuracy of the mixture with a 100 ppm concentration was 96%. When the concentration of the mixture was 100 ppm, the sensor array could recognize sixteen different xylene mixtures.

Recently, Gu *et al.* prepared ZnCar SURMOFs membranes with dynamic structural changes for selective recognition of six fragrance enantiomers ((+)/(−)-carvone, (+)/(−)-menthol,

Fig. 9 (a) Structures of monofunctional and difunctional terpenes and terpenoids. (b) Stern–Völmer plots of (−)-linalool added to 1-MONs. (c) Quenching percentage of fluorescence by (−)-linalool with exposure time in (S)-1-MONs-MMM and (R)-1-MONs-MMM. Reproduced with permission from ref. 38. Copyright 2021, American Chemical Society. (d) Radar plots of the responses of sensors exposed to five enantiomers. Reproduced with permission from ref. 69. Copyright 2021, Wiley-VCH.
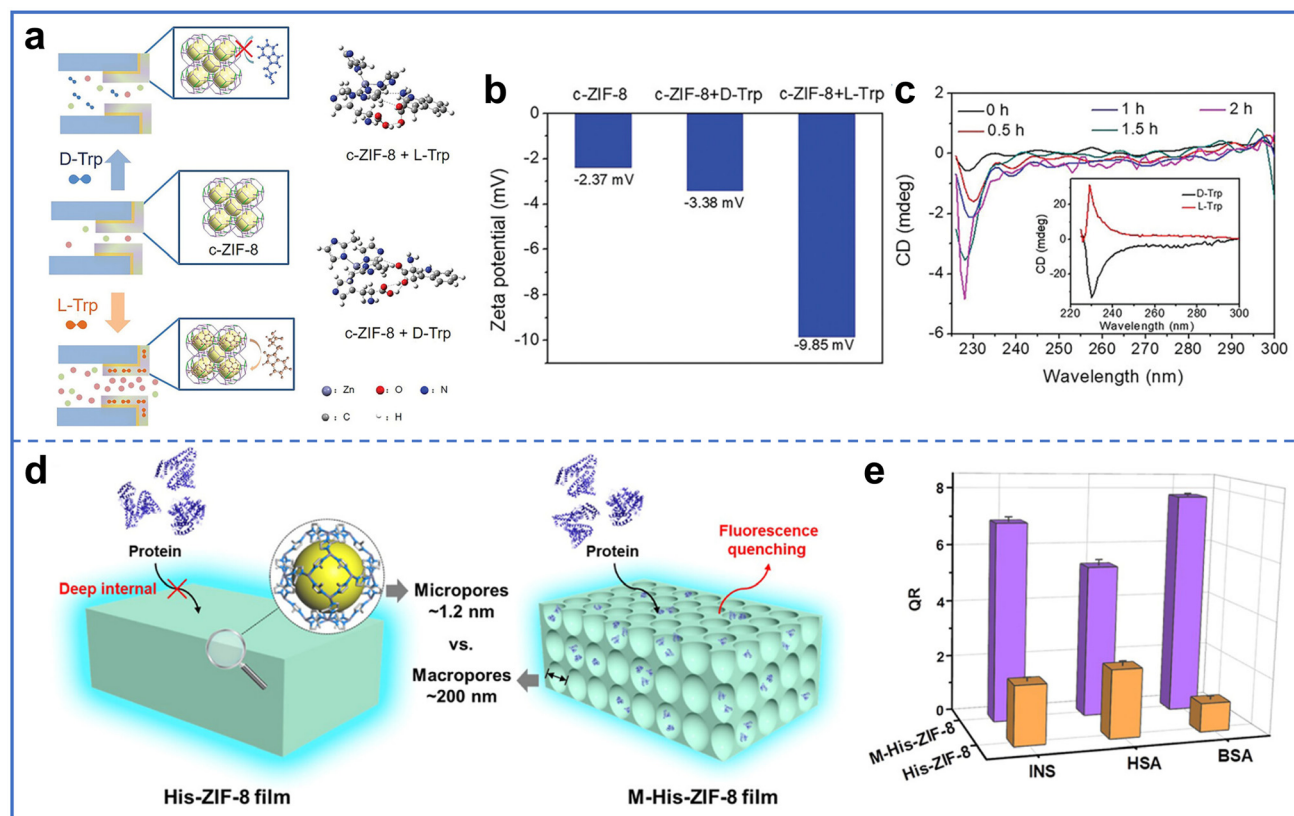
and (+)/(−)-limonene), mimicking the conformational changes of olfactory receptor proteins.[71] ZnCar SURMOFs were prepared using ligands of L-carnosine (Car) and Zn ions *via* the lbl method. A chiral sensor was constructed by integrating ZnCar SURMOFs into a QCM, achieving high recognition accuracy (98.58%) for fragrance enantiomers.

Electrochemical devices are widely used for chiral sensing due to their advantages of high sensitivity, high selectivity, low cost, and good stability.[72,73] Chiral MOFs can be deposited on electrodes for electrochemical chiral recognition.[74] For example, Zheng *et al.* immobilized chiral MOF nanofibers in chitosan (CS) to prepare a MOF/CS electrochemical sensor for selective detection of tyrosine (Tyr) enantiomers.[75] MOF and MOF/CS-modified glassy carbon electrodes (GCE) exhibited higher interfacial charge-transfer resistances than CS-modified GCEs, indicating that the introduction of CS improved electron transfer. Due to the synergistic effect of chiral MOF nanofibers and chiral CS, MOF/CS displayed the maximum peak current ratio, which was more sensitive for the detection of Tyr enantiomers. The concentrations of D/L-Tyr in the range of 0.007–0.055 mM were linearly correlated with the peak current of L/L-Tyr oxidation, demonstrating the quantitative detection of Tyr isomers. Compared with the initial current, the current loss after 10 days was only 8.9%, indicating that the MOF/CS

electrochemical sensor exhibits good repeatability and stability.

The chiral environment, such as nanoconfined spaces, has a significant impact on chiral recognition. Xia *et al.* revealed the influence of the chiral environment on chiral recognition by comparing the detection of three amino acids of enantiomers (tryptophan (Trp), Ala, and leucine (Leu)) with different sizes.[76] The dense chiral c-ZIF-8 layer was deposited on a gold-coated poly(ethylene terephtalate) (PET) nanochannel array using the cathodic deposition method, forming a c-ZIF-8-PET chiral membrane for electrochemical recognition. The selectivity is only found in enantiomers of Trp, among the three amino acids, as the chiral cavity size of c-ZIF-8 (8.1 Å) matched the molecular size of Trp but not Ala and Leu (Fig. 10a). After adding L-Trp, the zeta potential of c-ZIF-8 increased, while the zeta potential remained almost unchanged after adding D-Trp (Fig. 10b). This is attributed to the selective adsorption of negatively charged L-Trp molecules by the c-ZIF-8 layer, which increased the surface-charge density and led to an increase in the zeta potential. The continuous expansion of the D-Trp downward peak at 234 nm further indicated the sustained adsorption of L-Trp by c-ZIF-8 (Fig. 10c). The imidazole ring in D-Trp exhibits a steric hindrance effect, making it difficult to enter the chiral cavity of c-ZIF-8. The high adsorption capacity

Fig. 10 (a) Schematic of the interaction and adsorption differences between D-Trp and L-Trp with c-ZIF-8. (b) Zeta potential of the c-ZIF-8 membrane before and after the addition of D-Trp or L-Trp. (c) CD spectra of c-ZIF-8 after interaction with the Trp racemic mixture. Reproduced with permission from ref. 76. Copyright 2023, Wiley-VCH. (d) Different interactions of proteins with L-His-ZIF-8 membrane and M-L-His-ZIF-8 membrane. (e) Quenching ratio of M-His-ZIF-8 and His-ZIF-8 membranes after contact with INS, HSA, and BSA. Reproduced with permission from ref. 30. Copyright 2024, American Chemical Society.

of the c-ZIF-8 layer for L-Trp was beneficial for the interaction between L-Trp and chiral sites, thereby facilitating chiral recognition. The study indicated the important role of the size-matching effect in chiral recognition.

Typically, chiral MOF membranes have microporous structures in which biomolecules cannot easily enter, which makes the recognition of biomolecules challenging. To address this challenge, Cui *et al.* prepared a chiral MOF M-L-His-ZIF-8 membrane with hierarchical pores for detecting both small molecules and large proteins.[30] The chiral MOF M-L-His-ZIF-8 membrane enables highly selective detection of phenylethanol enantiomers. In detail, the fluorescence intensity of the membrane was significantly enhanced by (*R*)-phenylethanol but did not change with (*S*)-phenylethanol. The L-His part in MOFs interacted with the hydroxyl group in phenylethanol through hydrogen bonding, and the interaction between L-His-ZIF-8 and (*R*)-phenylethanol was stronger than that between (*S*)-phenylethanol.

Furthermore, the M-CMOF membrane with macropore and micropore structures exhibited excellent chiral recognition for proteins such as human serum albumin (HSA), bovine serum albumin (BSA), and insulin (INS) with high enantioselectivity (Fig. 10d and e). The M-L-His-ZIF-8 membrane retained the integrity of the macropore structure after 3 months and could be reused at least 5 times, indicating its excellent stability and recyclability.

Wearable smart biosensors for human health monitoring were also prepared using chiral MOF membranes. Xie *et al.* constructed flexible MMMs with RT@CDMOF and PES for wearable sensors to detect lactic acid in sweat and monitor fatigue levels during high-intensity exercise.[25] In RT@CDMOF, a dual response was achieved by encapsulation of both rhodamine 6G hydrazide (RGH) with fluorescence response and tetracyanovinylindane (TCN) with colorimetric response in γ-CDMOF. With the distinguishable color change and different affinity of L-lactic and D-lactic to MOF materials, RT@CDMOF MMMs exhibited rapid dual color sensing of lactic acid enantiomers with biocompatibility, flexibility, and mechanical stability, which was beneficial for health monitoring.

Chiral MOF membranes have been used for the recognition of various chemical enantiomers. The selective sensitivity was achieved by different interactions between the target molecules and chiral sites or structures. The various signal outputs, such as fluorescence and colorimetry, provide a diverse visual view. However, some improvements are still needed for chiral MOF membranes, *e.g.*, recognition ability of target molecules in
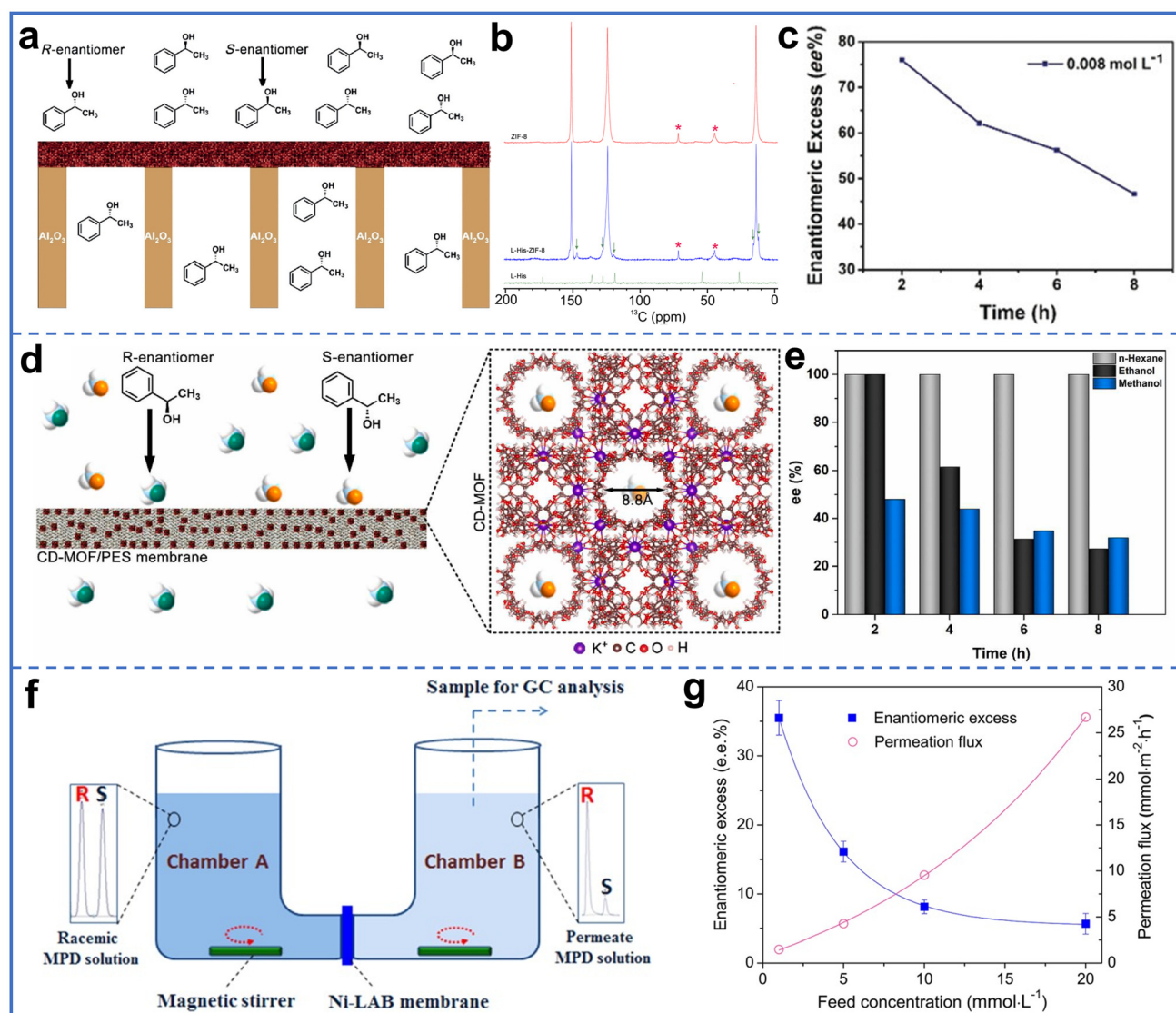
complex matrices and the stability of chiral MOF membranes in specific chemical or physical environments.

3.2. Separation

To avoid ineffective or even harmful effects from the enantiomer of a designed chiral material in drugs or food additives, it is significant to separate the enantiomers for a pure designed single configuration.[77,78] By designing pore structures and surface chemistry, chiral MOF membranes have also been successfully used for chiral enantiomer separation.[79,80]

Chiral alcohols are important precursors for the synthesis of chiral drugs.[81] Among them, 1-phenylethanol is widely

used. Specifically, S-1-phenylethanol is used for drugs to treat depression and asthma, while R-1-phenylethanol is a useful ophthalmic preservative and cholesterol adsorption inhibitor. Therefore, the separation of chiral enantiomers in 1-phenylethanol is of great significance. Wang et al. prepared an L-His-ZIF-8 membrane for the separation of racemic 1-phenylethanol (Fig. 11a).[19] L-His introduced a chiral environment into the MOF channel, thereby endowing the MOF with enantioselectivity. The peak shift of the membrane after permeation with 1-phenylethanol at 14 ppm and 124 ppm in solid-state nuclear magnetic resonance (NMR) indicated that the interaction between chiral molecules and MOF was very close at the

Fig. 11 (a) Schematic of the L-His-ZIF-8 membrane separating racemic 1-phenylethanol. (b) ^{13}C CPMAS NMR spectra of ZIF-8, L-His-ZIF-8, and L-His. (c) Enantiometric excess with time in separation of racemic 1-phenylethanol by L-His-ZIF-8 membrane. Reproduced with permission from ref. 19. Copyright 2018, Wiley-VCH. (d) Schematic of the separation of the 1-phenylethanol racemic mixture by CD-MOF/PES MMM. (e) Effect of solvents on separation of 1-phenylethanol racemates by MMMs. Reproduced with permission from ref. 53. Copyright 2021, Elsevier B.V. (f) Schematic of the separation of racemic MPD at low temperature through a Ni$_2$(L-asp)$_2$(bipy) membrane. (g) Enantiometric excess and permeation flux with feed concentrations at 30 °C in the separation of racemic MPD by Ni$_2$(L-asp)$_2$(bipy) membrane . Reproduced with permission from ref. 83. Copyright 2013, Wiley-VCH.

molecular level to the two sites in space (Fig. 11b). Due to the different interaction of S-1-phenylethanol and R-1-phenylethanol with L-His-ZIF-8, they permeated through the membrane at a difference rate, fulfilling the enantiomeric separation with an enantiometric excess (ee) value of 76% (Fig. 11c). The membrane separated the enantiomers three times without losing selectivity, and the crystal structure of L-His-ZIF-8 remained unchanged. To further improve the separation performance, they used chiral MIL-53-NH-L-His MMMs for separating racemic 1-phenylethanol at 100% ee.[44]

The same group also prepared CD-MOF/PES MMMs for the separation of racemic 1-phenylethanol with 100% ee (Fig. 11d).[53] In this study, the influence of solvent polarity on the separation performance was studied. The increase in solvent polarity led to a decrease in the enantioselectivity of the membrane, as polar solvents preferentially occupied chiral sites in MOFs, leading to reduced 1-phenylethanol adsorption in MOFs (Fig. 11e). In addition, chiral MOF membranes were assembled into a capillary column for the separation of racemic 1-phenylethanol. The chiral pillar-layered $Cu_2(D$-cam$)_2$P (D-cam was (1R,3S)-(+)-camphorate, P was 1,4-diazobicyclo[2.2.2] octane (dabco) and bipy) was grown layer by layer in a capillary column to form the membrane, which exhibited excellent separation efficiency for 1-phenylethanol.[82]
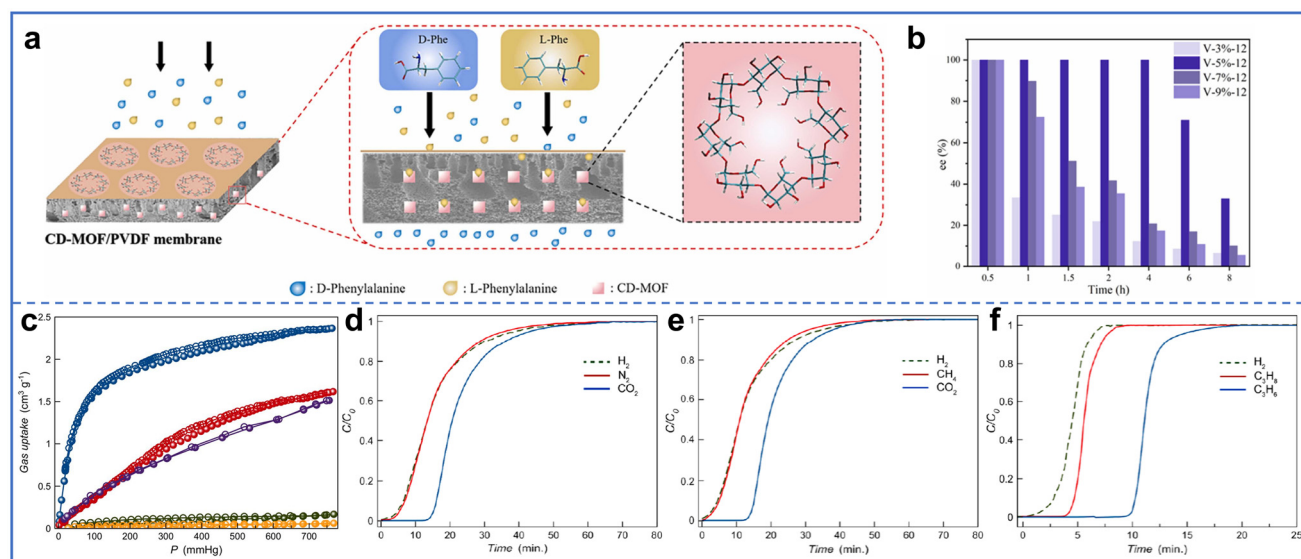
In addition to racemic 1-phenylethanol, 2-methyl-2,4-pentanediol (MPD), a type of dihydric alcohol, is an important intermediate in the synthesis of fine chemicals and chiral drugs. Qiu et al. prepared chiral $Ni_2(L$-asp$)_2$(bipy) membranes on nickel net via an in situ growth method for the separation of MPD isomer mixtures.[27] Due to the interaction between S-MPD and chiral channels in MOFs, (S)-MPD was adsorbed

on the active sites, whereas (R)-MPD had a higher permeability. The chiral $Ni_2(L$-asp$)_2$(bipy) membrane also exhibited excellent thermal stability in addition to the separation effect. Raising the separation temperature of the membrane from room temperature to 200 °C resulted in a higher permeability of R-MPD, leading to an ee value of 32.5% for racemic separation.

In the same year, Jin et al. reported the separation of MPD racemates at low temperatures using a $Ni_2(L$-asp$)_2$(bipy) membrane (Fig. 11f).[83] Unlike the preparation method reported by Qiu et al., they decreased the crystal size of the as-synthesized $Ni_2(L$-asp$)_2$(bipy) crystals by ball milling and then followed by secondary growth to form the membrane. R-MPD was more easily passed through a $Ni_2(L$-asp$)_2$(bipy) membrane with a higher permeability than S-MPD, achieving an ee value of approximately 35.5% at 30 °C (Fig. 11g).

Chiral 2,5-hexanediol (HDO) is another important precursor of chiral drugs and agricultural chemicals. It was successfully separated by chiral MOF membranes ($(\pm)$-[$\{Zn_2(cam)_2(dabco)\}_n$]).[84] The compatible size of HDO with the pores of MOFs and the hydrogen bond with the Zn-carboxylate groups in MOFs ensured the adsorption of HDO by MOFs. The separation of R-HDO and S-HDO was achieved by their different adsorption rates on the ($(\pm)$-[$\{Zn_2(cam)_2(dabco)\}_n$]) membranes.

Most drugs are racemate with enantiomers, and generally, only one enantiomer possesses therapeutic effects, whereas the other may be ineffective or cause side effects.[85] Yan et al. reported CD-MOF MMMs for the separation of phenylalanine (Phe) enantiomers with 100% separation efficiency (Fig. 12a).[86] When the load of CD-MOF in MMMs was 5%, the ee value reached the maximum (Fig. 12b). The ee was lower

Fig. 12 (a) Schematic of the separation of Phe enantiomers by CD-MOF MMMs. (b) Enantiometric excess with time in the separation of Phe enantiomers by CD-MOF MMMs. Reproduced with permission from ref. 86. Copyright 2023, Elsevier B.V. (c) Adsorption isotherms of C_3H_6 (blue), C_3H_8 (red), CO_2 (purple), CH_4 (black), and N_2 (yellow) at 298 K for activated $Cu_2^{II}(S,S)$-hismox·5H$_2$O. Experimental column breakthrough curves of (d) N_2/CO_2 (volume ratio was 75 : 25), (e) CH_4/CO_2 (volume ratio was 75 : 25), and (f) C_3H_6/C_3H_8 (volume ratio was 50 : 50) gas mixtures measured at 298 K and 1 bar. Reproduced with permission from ref. 89. Copyright 2019, American Chemical Society.

when the MOF loading was 3% because the CD-MOF content was too low to provide sufficient chiral recognition sites. The separation performance at CD-MOF loading levels of 7% and 9% was also lower than that at a loading level of 5% due to the aggregation of CD-MOF in the membrane, which led to the generation of defects in the membrane and decreased binding sites. The binding affinity between L-Phe and the chiral sites in CD-MOF was stronger, allowing it to adsorb in the membrane. D-Phe did not interact with the CD-MOF and preferentially passed through the membrane to achieve the chiral separation of Phe enantiomers.

In addition, chiral MOF membranes can also be used to separate naproxen to obtain S-naproxen with pain relief and anti-inflammatory effects.[23] Compared with S-naproxen, R-naproxen exhibited a stronger affinity with chiral MOF-808. When enantiomers passed through the membrane, R-naproxen underwent noncovalent interaction with chiral MOFs within the membrane, whereas S-naproxen preferentially permeated through the membrane. The molecular dynamics simulation showed almost no significant difference in the diffusion rates of the two enantiomers in MOF-808, whereas the diffusivity of S-naproxen in chiral MOF-808 was higher than that of R-naproxen. The chiral MOF-808-Ala obtained from L-Ala post-modification showed an ee value of approximately 95.0%. Due to the excellent structural stability of chiral MOF-808, the membrane exhibited good integrity after separation.

The separation of ibuprofen enantiomers is significant because S-(+)-ibuprofen is 160 times more pharmacologically active than R-(−)-ibuprofen and is more easily to be metabolized. Ben et al. prepared chiral (P)-CoMOF membranes by symmetrical breaking in ligand dimethyl pyridine-2,5-dicarboxylate and cobalt ions.[87] Efficient separation of ibuprofen enantiomers (100% ee) was achieved according to the different adsorption and desorption rates of S-(+)-ibuprofen and R-(−)-ibuprofen on (P)-CoMOF membrane.

Chiral MOF membranes are also used for the separation of gas mixtures due to their differences in interactions with different gas molecules. Jin et al. prepared chiral $[Ni_2(mal)_2(bpy)]\cdot 2H_2O$ membrane for the selective separation of H_2/CO_2.[88] The ideal selectivity of H_2/CO_2 was calculated to be 89 based on the permeability of the membrane to H_2 and CO_2. Due to the significant quadrupole moment and polarizability, the strong interaction between CO_2 and the chiral MOF frameworks resulted in powerful adsorption onto the membrane. The lower permeability of CO_2 compared to H_2 led to excellent H_2/CO_2 separation of the chiral MOF membrane.

Pardo et al. achieved the separation of gas mixtures including natural gas, flue gas, and petrochemical industrial gas using a chiral MOF membrane.[89] The chiral $Cu_2^{II}(S,S)$-hismox·$5H_2O$ (hismox was bis[(S)-histidine]oxalyl diamide) was dispersed into poly(ether-co-amide) multiblock copolymer to prepare the MMMs as the stationary phase for the chromatographic column, achieving the separation of CO_2/N_2, CO_2/CH_4, and C_3H_8/C_3H_6 gas mixtures. The chiral MOFs possessed significant adsorption capacity for CO_2, C_3H_8, and C_3H_6, but almost no adsorption capacity for CH_4 and N_2, indicating their potential for separating gas mixtures (Fig. 12c–f). The noninteracting channels were formed with MOFs, which preferentially passed through the membrane, consistent with the poor adsorption of CH_4 and N_2 by MOFs. This chiral MOF membrane enabled the separation of gas mixtures for economical or environmental values.

The separation of chiral drug precursors, drug molecules, and gas molecules was achieved by chiral MOF membranes through distinguishable absorption or desorption rates of enantiomers from the membranes. Compared to traditional chromatographic separation, chiral MOF membrane separation has the advantages of low energy consumption, easy adjustment of pore size and functional groups, and large-scale separation. However, more types of high-quality chiral MOF membranes still need to be developed for higher separation efficiency, adaptability for a broader range of enantiomers and mechanical research.
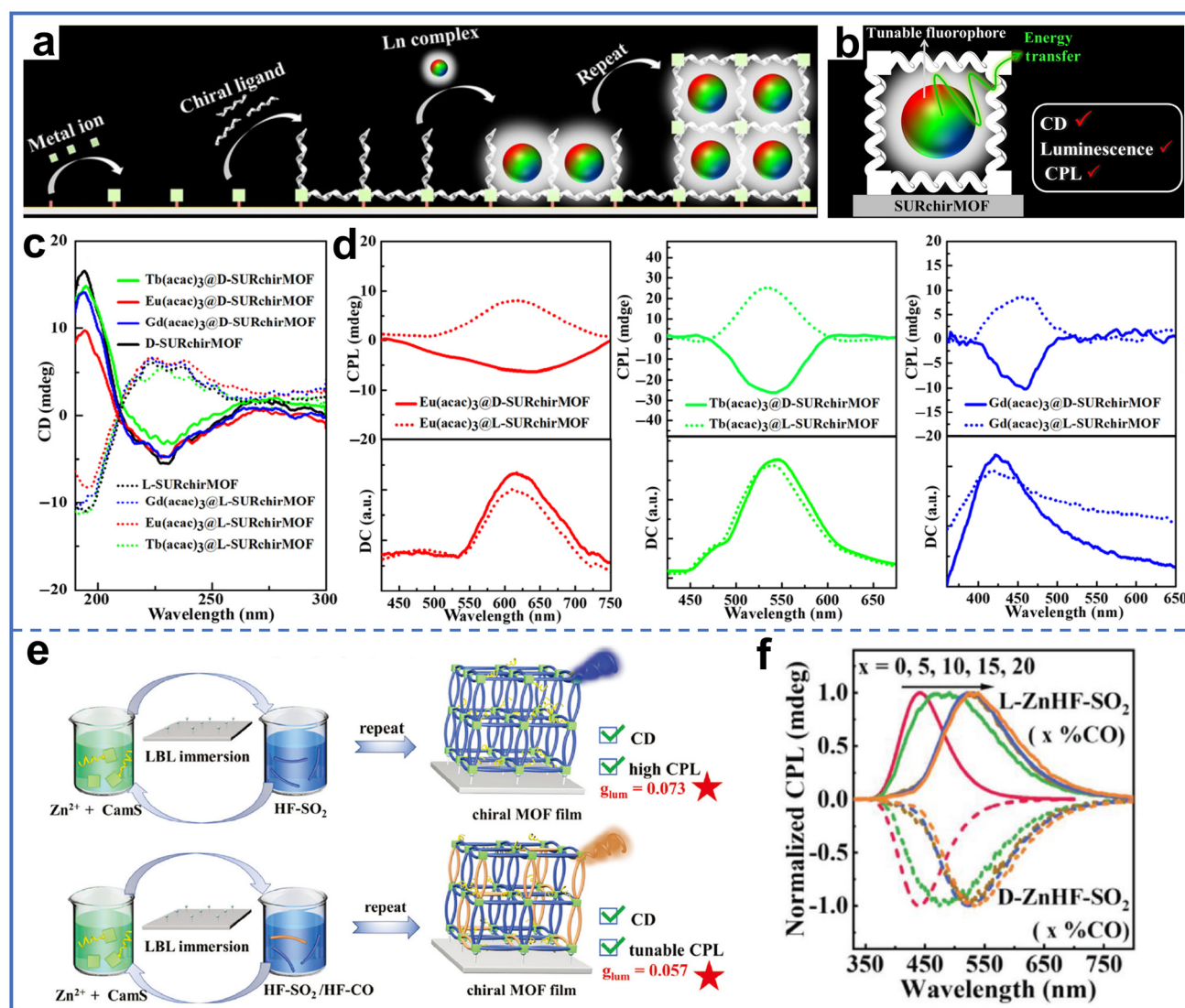
3.3.   Circularly polarized luminescence

CPL refers to left-handed or right-handed circularly polarized luminescence, and it has broad application prospects in fields such as 3D displays, chiral recognition, information storage, and optoelectronic devices.[90] MOF materials are ideal chiral luminophores because their specific porous structures provide multiple routes for chiral emission, including chiral units on the MOF blocks and in the pores.[91]

Gu et al. encapsulated the lanthanide complexes $Ln(acac)_3$ (acac was acetylacetone) into the pores of chiral MOF $[Zn_2(cam)_2dabco]_n$ to obtain $Ln(acac)_3$@SURchirMOF membrane with excellent CPL property (Fig. 13a).[92] The lanthanide complexes $Eu(acac)_3$, $Tb(acac)_3$, and $Gd(acac)_3$ emitted primary red, green, and blue light under ultraviolet irradiation, respectively. The chiral MOFs with weak photoluminescent emission in the membrane hardly affected the photoluminescent emission of the lanthanide complexes. The chirality of the MOFs was maintained after the encapsulation of $Ln(acac)_3$, as indicated by the same circular dichroism (CD) signals (Fig. 13c). The $Ln(acac)_3$@SURchirMOF membrane exhibited a photoluminescent emission similar to that of $Ln(acac)_3$, thereby achieving the tunable CPL of the membrane (Fig. 13d). The increase in the fluorescent lifetime of chiral MOFs in the membrane and the decrease in fluorescent lifetime of lanthanide complexes indicated energy transfer from $Ln(acac)_3$ to chiral MOFs, where $Ln(acac)_3$ acted as the donor and chiral MOFs acted as the acceptor. The encapsulation of lanthanide complexes in chiral MOF pores was crucial for achieving CPL property, as the coordination or intermolecular interactions between acac in the complex and Zn nodes in the MOF resulted in efficient energy transfer (Fig. 13b).

Another method to endow MOF membranes with CPL properties is to encapsulate chiral molecules into luminescent MOF membranes. Zhang's group prepared luminescent MOF membranes using the lbl spraying method and then loaded chiral molecules into the pores of MOFs to endow the membrane with CPL properties.[93] The molecule 4,4′-(1,2-dipheny-

Fig. 13 (a) Schematic of the preparation of Ln(acac)₃@SURchirMOF membrane by encapsulating the Ln complex into chiral MOF pores. (b) Schematic of energy transfer in the host–guest membrane of Ln(acac)₃@SURchirMOFs. (c) CD spectra of Ln(acac)₃@SURchirMOFs and chiral MOFs. (d) CPL spectra of Ln(acac)₃@SURchirMOFs. Reproduced with permission from ref. 92. Copyright 2022, Springer Nature. (e) Preparation of D/L-ZnHF-SO₂ membranes and D/L-ZnHF-SO₂/COmembranes by lbl chiral induction method. (f) Normalized CPL spectra of D/L-ZnHF-SO₂ (*x*% CO represented the proportion of HF-CO ligands) membranes. Reproduced with permission from ref. 94. Copyright 2024, Wiley-VCH.

lethene-1,2-diyl) dibenzoic acid (TPE) with aggregation-induced emission was used as the ligand to self-assemble with Zn ions *via* the lbl method, resulting in a ZnTPE membrane with photoluminescence. Then, chiral dibenzoyl-tartaric acid was loaded into the pores of ZnTPE *via* a post modification method. The fluorescence emission of the MOF membrane loaded with chiral molecules maintained strong fluorescence with a shift from 495 to 478 nm. The membrane exhibited a uniform CPL signal due to the π–π conjugation effect between the benzene ring of the loaded chiral molecule and ZnTPE.

In addition, the same group also prepared chiral D/L-ZnHF-SO₂ (HF-SO₂ was 3,7-dibenzothiophenedicarboxylate, 5,5-dioxide) membranes using camphorsulfonic acid as a chiral inductor *via* the lbl chiral induction method (Fig. 13e).[94] The ZnHF-SO₂ membranes exhibited strong CPL properties,

with the CPL signal appearing at 440 nm, consistent with the fluorescent emission of the membranes. The 9-fluororenone-2,7-dicarboxylate (HF-CO) molecule has a similar structure to the HF-SO₂ ligand in MOFs and can therefore be introduced as a mixed ligand to prepare photoluminescent MOFs. By adjusting the proportion of ligands, CPL colors in the MOF membranes could be modulated (Fig. 13f). The membranes with different ligand ratios exhibited CPL signals at different positions due to energy transfer between HF-SO₂ ligands and Zn ions and between Zn ions and HF-CO ligands.

Furthermore, Zhang's group crosslinked CLC with MOFs to prepare a CLCMOF membrane for achieving CPL performance in photo-thermal switching, which was used for information anticounterfeiting and encryption.[58] CLC was a thermally induced liquid crystal that gradually changed from an amor-

Table 1 Compositions and applications of chiral MOF membranes

	MOF materials	Matrices	Applications
Pure chiral MOF membranes	$Ni_2(L\text{-asp})_2(bipy)$		Separation of racemic MPD[27]
	L-His-ZIF-8		Separation of racemic 1-phenylethanol[19]
	MOF-808-Ala, MOF-808-Thr, MOF-808-His		Separation of racemic naproxen enantiomers[23]
	$Cu_2(DCam)_2(AzoBiPyB)$		Enantiopure uptakes of racemic phenylethanol[28]
	γCD-SURMOF		Recognition and separation of enantiomeric tripeptide pair[29]
	His-ZIF-8, $[Cd(LTP)_2]_n$, $[Cu(mal)bpy]\cdot H_2O$		Recognition of racemic phenylethanol, HAS, BSA, or INS[30]
	Meso-L-CuMOF		Recognition of monosaccharide enantiomers[64]
	$Cu_2(DCam)_2(dabco)$, $Cu_2(DCam)_2(BiPy)$, $Cu_2(DCam)_2(BiPyB)$, HKUST-1, Cu(BDC), Cu(BPDC)		Recognition of limonene, 2-octanol, 1-phenylethanol, 1-phenylethylamine, or methyl lactate enantiomers[69]
	c-ZIF-8		Detection of Trp, Ala, and Leu enantiomers[76]
	$Cu_2(D\text{-cam})_2P$		Separation of racemic 1-phenylethanol[82]
	$Ni_2(L\text{-asp})_2(bipy)$		Separation of racemic MPD at low temperatures[83]
	$[Ni_2(mal)_2(bpy)]\cdot 2H_2O$		Separation of H_2/CO_2[88]
	$Ln(acac)_3$@SURchirMOF		CPL performance[92]
	ZnTPE		CPL luminescence performance[93]
	$D/L\text{-ZnHF-SO}_2$		CPL properties[94]
MMMs	RT@CDMOF	PES	Recognition of lactic acid enantiomers[25]
	MIL-53-NH-L-His	PES	Separation of racemic 1-phenylethanol[44]
	γ-CD-MOF	PES	Separation of racemic 1-phenylethanol[53]
	Zn-BLD	HDPE and UHMWPE	Separation of racemic methyl phenyl sulfoxide[55]
	$Zn_2(sdc)_2$	CLC	Information encryption of Morse code[58]
	D-Met@MOF	MPN	Anti-biofouling efficacy[59]
	$[Cu_2((+)\text{-Cam})_2Dabco]_n$, $[Cu_2((+)\text{-Cam})_2Bipy]_n$	Poly(dopamine) and polycarbonate trail etched membrane	Separation of racemic 1-phenylethanol[62]
	1-MONs	PES	Sensing of terpenes and terpenoids[38]
	L-His&R6G@ZIF-8	PVDF	Sensing of proline enantiomers[54]
	MOF nanofibers	CS	Electrochemical sensing of Tyr isomers[75]
	$Eu(BTC)(H_2O)\cdot DMF$	PIM-1	Separation of 2-amino-1-butanol enantiomers[79]
	CD-MOF	PVDF	Separation of Phe enantiomers[86]
	$Cu^{II}_2(S,S)\text{-hismox}\cdot 5H_2O$	Poly(ether-co-amide) multiblock copolymer	Separation of CO_2/N_2, CO_2/CH_4, and C_3H_8/C_3H_6[89]

phous solid-like state to a transparent liquid state with increasing temperature, and the transmittance of the membrane also increased with increasing temperature. The UV–vis spectra of the CLCMOF membrane are consistent with the MOF membrane loaded with CLC without cycloaddition reaction, indicating that the CLCMOF membrane retained photochromic properties. The S-LCMOF membrane selectively reflected right-handed circularly polarized light and transmitted left-handed circularly polarized light, while the R-LCMOF membrane was the opposite. When the membrane was heated at 140 °C and irradiated with UV, the CPL changed from yellow to blue fluorescence. Since the photoluminescence and CPL signals of the CLCMOF membrane were regulated through irradiation and heating, molecular logic gates were designed for Morse code information encryption.

Chiral MOF membranes have been proven an ideal platform for CPL development due to their diverse structures and helical channels. Long-range periodic stacking in chiral MOF membranes is advantageous for the improvement of photoluminescence quantum yield and asymmetric factor. In addition, guest luminescent materials with different wavelengths are easy to be encapsulated into chiral MOFs for color-ful CPLs. In the future, organic ligands or metal ions with specific chiral centers and coordination geometries are expected to be introduced for more efficient chiral transfer and CPL.

Table 1 summarizes MOF materials and matrices used for chiral MOF membranes, as well as their applications.

4. Conclusions and outlook

Chiral MOF membranes show great potential for chiral recognition or separation and chiral emission due to their porous structure and simplicity of functionalization. In this review, we first summarized the various methods for synthesizing chiral MOF membranes, including direct methods for preparing pure chiral MOF membranes (e.g. solvothermal synthesis, lbl synthesis, and template-assisted synthesis) and indirect methods for fabricating chiral MOF MMMs (e.g. solution casting and TIPS-HoP). Pure chiral MOF membranes contain a high density of functional sites, whereas MMMs exhibit excellent flexibility and stability.

Second, we summarized the applications of chiral MOF membranes in chiral sensing, separation, and CPL. Chiral MOF membranes have been used in chiral sensing and separation of various molecules with high detectivity and selectivity. Membranes that combine photoluminescent units with chiral MOFs, or chiral molecules with luminescent MOFs, exhibit tunable CPL, indicating potential applications in imaging, optoelectronic devices, information anticounterfeiting and encryption.

However, the successful applications of chiral MOF membranes are still limited, which can be attributed to the challenges associated with the fabrication of high-quality membranes despite the abundance of chiral MOF materials. To improve the quality of chiral MOF membranes, research efforts can be directed towards the following areas.

From the perspective of MOF materials, the exploration of functional groups, such as groups with chirality or catalytic sites, is important to broaden their applications. In addition, stable ligands and metal ions should be selected to improve the stability of chiral MOFs. Furthermore, synthesis methods and conditions, such as the metal-ion-to-organic-ligand ratio, should be creatively modified to optimize the size of the MOF particles.

From the perspective of membranes, the interface between MOF particles and the matrix in MMMs is a key concern. To produce high-quality membranes (defect-free, uniform, and dense), the MOF materials must be compatible with the polymer matrix. Thus, the functional groups on organic ligands in chiral MOFs and matrices should be carefully selected to promote covalent or coordination interactions. In addition, the introduction of specific functional groups, such as hydrophobic groups and corrosion-resistant groups, should be considered to enhance water resistance and chemical stability. Furthermore, membrane preparation techniques, such as electrochemical deposition and microwave-assisted methods, should be broadened to develop better and multifunctional membranes.

Chiral MOF membranes, as emerging functional materials, have demonstrated excellent performance in chiral recognition and luminescence. With further improvements in quality and functional investigations, chiral MOF membranes are expected to play a more important role in these fields.

Author contributions

Yun Fan conceived and wrote the manuscript. Mengyun Chen conceptualized and revised the review.

Data availability

No primary research results, software or code has been included, and no new data were generated or analyzed as part of this review.

Conflicts of interest

The authors declare no conflicts of interest.

Acknowledgements

References

1 H. Furukawa, K. E. Cordova, M. O'Keeffe and O. M. Yaghi, *Science*, 2013, **341**, 1230444.

2 G. Lu, S. Li, Z. Guo, O. K. Farha, B. G. Hauser, X. Qi, Y. Wang, X. Wang, S. Han, X. Liu, J. S. DuChene, H. Zhang, Q. Zhang, X. Chen, J. Ma, S. C. J. Loo, W. D. Wei, Y. Yang, J. T. Hupp and F. Huo, *Nat. Chem.*, 2012, **4**, 310–316.

3 J. Guo, Y. Qin, Y. Zhu, X. Zhang, C. Long, M. Zhao and Z. Tang, *Chem. Soc. Rev.*, 2021, **50**, 5366–5396.

4 Q. Zhou, Q. Ding, Z. Geng, C. Hu, L. Yang, Z. Kan, B. Dong, M. Won, H. Song, L. Xu and J. S. Kim, *Nano-Micro Lett.*, 2025, **17**, 50.

5 J. He, X. Wen, L. Wu, H. Chen, J. Hu and X. Hou, *TrAC, Trends Anal. Chem.*, 2022, **156**, 116715.

6 Z. Huang, X. Shen, Y. Wei, J. W. Chew, E. H. Ang and M. Pan, *Mater. Horiz.*, 2024, **11**, 6098–6106.

7 Y. Wang, N. Wu, Y. Wang, H. Ma, J. Zhang, L. Xu, M. K. Albolkany and B. Liu, *Nat. Commun.*, 2019, **10**, 2500.

8 Z. Liu, J. Ai, T. Bai, Y. Fang, K. Ding, Y. Duan, L. Han and S. Che, *Chem*, 2022, **8**, 186–196.

9 J. E. Rekoske, *AIChE J.*, 2001, **47**, 2–5.

10 D. S. Bradshaw, J. M. Leeder, M. M. Coles and D. L. Andrews, *Chem. Phys. Lett.*, 2015, **626**, 106–110.

11 X. Su, J. Sun, J. Liu, Y. Wang, J. Wang, W. Tang and J. Gong, *Angew. Chem., Int. Ed.*, 2024, **63**, e202402886.

12 N. Chhabra, M. L. Aseri and D. Padmanabhan, *Int. J. Appl. Basic Med. Res.*, 2013, **3**, 16–18.

13 C. D. Wu, A. Hu, L. Zhang and W. B. Lin, *J. Am. Chem. Soc.*, 2005, **127**, 8940–8941.

14 Z. Sharifzadeh, S. A. A. Razavi and A. Morsali, *Green Chem.*, 2023, **25**, 8661–8678.

15 M. Zhang, Z.-J. Pu, X.-L. Chen, X.-L. Gong, A.-X. Zhu and L.-M. Yuan, *Chem. Commun.*, 2013, **49**, 5201–5203.

16 Z. Gu, Y. Luo, X. Zhang, Z. Zhu, Y. Wang, T. Tang, S. Zhang and W. Zhang, *TrAC, Trends Anal. Chem.*, 2024, **179**, 117864.

17 H.-J. Choi and D.-Y. Koh, *Membranes*, 2022, **12**, 357.

18 T. Duerinck and J. F. M. Denayer, *Chem. Eng. Sci.*, 2015, **124**, 179–187.

19 J. Y. Chan, H. Zhang, Y. Nolvachai, Y. Hu, H. Zhu, M. Forsyth, Q. Gu, D. E. Hoke, X. Zhang, P. J. Marriot and H. Wang, *Angew. Chem., Int. Ed.*, 2018, **57**, 17130–17134.

20 J. Liang, Y. Song, H. Xing, L. Ma, F. Wang, M. Zhang, H. Zhang, G. Zou and G. Yang, *Nanoscale*, 2024, **16**, 22011–22020.

21 Y.-H. Xiao, Z.-Z. Ma, X.-X. Yang, D.-S. Li, Z.-G. Gu and J. Zhang, *ACS Nano*, 2023, **17**, 19136–19143.

22 W. Wang, X. Dong, J. Nan, W. Jin, Z. Hu, Y. Chen and J. Jiang, *Chem. Commun.*, 2012, **48**, 7022–7024.

23 T. Chen, H. Li, X. Shi, J. Imbrogno and D. Zhao, *J. Am. Chem. Soc.*, 2024, **146**, 14433–14438.

24 H.-J. Choi, Y.-H. Ahn and D.-Y. Koh, *Membranes*, 2021, **11**, 279.

25 X.-L. Yang, Z.-Y. Yang, R. Shao, R.-F. Guan, S.-L. Dong and M.-H. Xie, *Adv. Mater.*, 2023, **35**, 2304046.

26 J. He, J. He, L. Tang, Y. Xia, J. Zhou, X. Jiang and X. Hou, *TrAC, Trends Anal. Chem.*, 2024, **175**, 117709.

27 Z. Kang, M. Xue, L. Fan, J. Ding, L. Guo, L. Gao and S. Qiu, *Chem. Commun.*, 2013, **49**, 10569–10571.

28 A. B. Kanj, J. Buerck, S. Grosjean, S. Braese and L. Heinke, *Chem. Commun.*, 2019, **55**, 8776–8779.

29 L.-M. Chang, Q.-h. Li, P. Weidler, Z.-G. Gu, C. Wöll and J. Zhang, *CCS Chem.*, 2022, **4**, 3472–3481.

30 J. Yang, Q. Song, T. Zhang, Y. Yan, C. Yuan, Y. Cui and X. Hou, *Anal. Chem.*, 2024, **96**, 17280–17289.

31 X. Liang, F. Zhang, W. Feng, X. Zou, C. Zhao, H. Na, C. Liu, F. Sun and G. Zhu, *Chem. Sci.*, 2013, **4**, 983–992.

32 L. A. Hall, D. M. D'Alessandro and G. Lakhwani, *Chem. Soc. Rev.*, 2023, **52**, 3567–3590.

33 M. Ma, J. Chen, H. Liu, Z. Huang, F. Huang, Q. Li and Y. Xu, *Nanoscale*, 2022, **14**, 13405–13427.

34 Z. F. Chen, J. Zhang, R. G. Xiong and X. Z. You, *Inorg. Chem. Commun.*, 2000, **3**, 493–496.

35 N. Corella-Ochoa, J. B. Tapia, H. N. Rubin, V. Lillo, J. González-Cobos, J. Luis Núñez-Rico, S. R. G. Balestra, N. Almora-Barrios, M. Lledós, A. Güell-Bara, J. Cabezas-Giménez, E. C. Escudero-Adán, A. Vidal-Ferran, S. Calero, M. Reynolds, C. Martí-Gastaldo and J. Ramón Galán-Mascarós, *J. Am. Chem. Soc.*, 2019, **141**, 14306–14316.

36 M. P. Yutkin, M. S. Zavakhina, D. G. Samsonenko, D. N. Dybtsev and V. P. Fedin, *Inorg. Chim. Acta*, 2013, **394**, 367–372.

37 K. Tanaka, D. Yanamoto, K. Yoshimura, T. Anami and Z. Urbanczyk-Lipkowska, *CrystEngComm*, 2015, **17**, 1291–1295.

38 Y. Liu, L. Liu, X. Chen, Y. Liu, Y. Han and Y. Cui, *J. Am. Chem. Soc.*, 2021, **143**, 3509–3518.

39 K. Berijani and A. Morsali, *J. Catal.*, 2019, **378**, 28–35.

40 P. Cui, P. Wang, Y. Zhao and W.-Y. Sun, *Cryst. Growth Des.*, 2019, **19**, 1454–1470.

41 Z. Han, K. Wang, Y. Guo, W. Chen, J. Zhang, X. Zhang, G. Siligardi, S. Yang, Z. Zhou, P. Sun, W. Shi and P. Cheng, *Nat. Commun.*, 2019, **10**, 5117.

42 W.-T. Kou, C.-X. Yang and X.-P. Yan, *J. Mater. Chem. A*, 2018, **6**, 17861–17866.

43 G. Yang, W. Shi, Y. Qian, X. Zheng, Z. Meng and H.-L. Jiang, *Angew. Chem., Int. Ed.*, 2023, **62**, e202308089.

44 Y. Lu, H. Zhang, J. Y. Chan, R. Ou, H. Zhu, M. Forsyth, E. M. Marijanovic, C. M. Doherty, P. J. Marriott, M. M. B. Holl and H. Wang, *Angew. Chem., Int. Ed.*, 2019, **58**, 16928–16935.

45 C. Tan, X. Han, Z. Li, Y. Liu and Y. Cui, *J. Am. Chem. Soc.*, 2018, **140**, 16229–16236.

46 B. Vilhanová, M. Ranocchiari and J. A. van Bokhoven, *ChemCatChem*, 2016, **8**, 308–312.

47 A. B. Kanj, J. Buerck, N. Vankova, C. Li, D. Mutruc, A. Chandresh, S. Hecht, T. Heine and L. Heinke, *J. Am. Chem. Soc.*, 2021, **143**, 7059–7068.

48 J.-S. Feng, M. Ren, Z.-S. Cai, K. Fan, S.-S. Bao and L.-M. Zheng, *Chem. Commun.*, 2016, **52**, 6877–6880.

49 T. Yamada, T. Eguchi, T. Wakiyama, T. Narushima, H. Okamoto and N. Kimizuka, *Chem. – Eur. J.*, 2019, **25**, 6698–6702.

50 S.-T. Wu, Z.-W. Cai, Q.-Y. Ye, C.-H. Weng, X.-H. Huang, X.-L. Hu, C.-C. Huang and N.-F. Zhuang, *Angew. Chem., Int. Ed.*, 2014, **53**, 12860–12864.

51 J. Zhang, S. Chen, R. A. Nieto, T. Wu, P. Feng and X. Bu, *Angew. Chem., Int. Ed.*, 2010, **49**, 1267–1270.

52 D. Wu, K. Zhou, J. Tian, C. Liu, J. Tian, F. Jiang, D. Yuan, J. Zhang, Q. Chen and M. Hong, *Angew. Chem., Int. Ed.*, 2021, **60**, 3087–3094.

53 Y. Lu, J. Y. Chan, H. Zhang, X. Li, Y. Nolvachai, P. J. Marriott, X. Zhang, G. P. Simon, M. M. B. Holl and H. Wang, *J. Membr. Sci.*, 2021, **620**, 118956.

54 Y.-H. Geng, Y. Xin, J. Du, M.-Y. Cui, Y.-Y. Liu, L.-X. Zhang and B. Ding, *Spectrochim. Acta, Part A*, 2024, **305**, 123468.

55 H. Wang, S. Zhao, Y. Liu, R. Yao, X. Wang, Y. Cao, D. Ma, M. Zou, A. Cao, X. Feng and B. Wang, *Nat. Commun.*, 2019, **10**, 4204.

56 B. D. Freeman, *Macromolecules*, 1999, **32**, 375–380.

57 L. M. Robeson, *J. Membr. Sci.*, 2008, **320**, 390–400.

58 X.-X. Yang, N. Li, C. Li, Z.-B. Jin, Z.-Z. Ma, Z.-G. Gu and J. Zhang, *J. Am. Chem. Soc.*, 2024, **146**, 16213–16221.

59 Z. Yu, X. Li, Z. Wang, Y. Fan, W. Zhao, D. Li, D. Xu, T. Gu and F. Wang, *Adv. Mater.*, 2024, **36**, 2407409.

60 C. Li and L. Heinke, *Symmetry*, 2020, **12**, 686.

61 X. Niu, M. Yuan, X. Yang, H. Li, R. Zhao, Y. Liu, H. Zhao and K. Wang, *ACS Appl. Nano Mater.*, 2024, **7**, 19175–19183.

62 M. Chen, X. Li, J. Li, C. Liu, A. Yu and S. Zhang, *Sep. Purif. Technol.*, 2024, **331**, 125704.

63 L. Geng, Y. Qiao, R. Sun, L. Guo, Z.-Q. Li, Y. Ma, M.-H. Yu, Z. Chang and X.-H. Bu, *Adv. Mater.*, 2025, **37**, 2415511.

64 J. Guo, X. Liu, J. Zhao, H. Xu, Z. Gao, Z.-Q. Wu and Y.-Y. Song, *Chem. Sci.*, 2023, **14**, 1742–1751.

65 X. Niu, R. Zhao, Y. Liu, M. Yuan, H. Zhao, H. Li, X. Yang, H. Xu and K. Wang, *J. Mater. Chem. A*, 2023, **11**, 23376–23386.

66 J.-Y. Liu, Y.-H. Geng, T.-T. Wang, B. Ding, Y.-H. Qiao, J.-Z. Huo and B. Ding, *ACS Appl. Nano Mater.*, 2023, **6**, 398–409.

67 Y.-W. Zhao, L.-E. Guo, F.-Q. Zhang, J. Yao and X.-M. Zhang, *ACS Appl. Mater. Interfaces*, 2021, **13**, 20821–20829.

68 Y. Zhang, Y. Wang, Y. Dai, X. Bai, X. Hu, L. Du, H. Hu, X. Yang, D. Li, Q. Dai, T. Hasan and Z. Sun, *Sci. Adv.*, 2022, **8**, eabq8246.

69 S. Okur, P. Qin, A. Chandresh, C. Li, Z. Zhang, U. Lemmer and L. Heinke, *Angew. Chem., Int. Ed.*, 2021, **60**, 3566–3571.

70 P. Qin, B. A. Day, S. Okur, C. Li, A. Chandresh, C. E. Wilmer and L. Heinke, *ACS Sens.*, 2022, **7**, 1666–1675.

71 N. Li, J.-B. Zhang, C. Woell, Z.-G. Gu and J. Zhang, *Adv. Funct. Mater.*, 2025, 2422860.

72 L. Lan, X. Kuang, X. Sun, Q. Wei and R. Kuang, *Anal. Chem.*, 2023, **95**, 18295–18302.

73 X. Niu, S. Yan, R. Zhao, H. Li, X. Liu and K. Wang, *ACS Appl. Mater. Interfaces*, 2023, **15**, 22435–22444.

74 X. Niu, Y. Liu, R. Zhao, M. Yuan, H. Zhao, H. Li and K. Wang, *ACS Appl. Mater. Interfaces*, 2024, **16**, 17361–17370.

75 L. Tong, X. Kuang, Q. Duan and X. Zheng, *Starke*, 2021, **73**, 2100112.

76 M.-Y. Wu, R.-J. Mo, X.-L. Ding, L.-Q. Huang, Z.-Q. Li and X.-H. Xia, *Small*, 2023, **19**, 2301460.

77 F. Wang, K. He, R. Wang, H. Ma, P. J. Marriott, M. R. Hill, G. P. Simon, M. M. B. Holl and H. Wang, *Adv. Mater.*, 2024, **36**, 2400709.

78 G. Sun, Y. Luo, Z. Yan, H. Qiu and W. Tang, *Chin. Chem. Lett.*, 2024, **35**, 109787.

79 S. Das, S. Xu, T. Ben and S. Qiu, *Angew. Chem., Int. Ed.*, 2018, **57**, 8629–8633.

80 Y. Duan, L. Li, Z. Shen, J. Cheng and K. He, *Membranes*, 2023, **13**, 480.

81 Z.-J. Li, J. Yao, Q. Tao, L. Jiang and T.-B. Lu, *Inorg. Chem.*, 2013, **52**, 11694–11696.

82 Z.-G. Gu, W.-Q. Fu, X. Wu and J. Zhang, *Chem. Commun.*, 2016, **52**, 772–775.

83 K. Huang, X. Dong, R. Ren and W. Jin, *AIChE J.*, 2013, **59**, 4364–4372.

84 B. Liu, O. Shekhah, H. K. Arslan, J. Liu, C. Woell and R. A. Fischer, *Angew. Chem., Int. Ed.*, 2012, **51**, 807–810.

85 F. Zhang, L. He, W. Sun, Y. Cheng, J. Liu and Z. Ren, *RSC Adv.*, 2015, **5**, 41729–41735.

86 Q. Ye, J. Li, Y. Huang, H. Wu, Y. Li and B. Yan, *J. Environ. Chem. Eng.*, 2023, **11**, 109250.

87 B. Li, Y. Feng, D. Zhou, M. Yang, D. Li, S. Zhang, J. Fu and T. Ben, *J. Mater. Chem. A*, 2025, **13**, 8375–8384.

88 Q. Li, G. Liu, K. Huang, J. Duan and W. Jin, *Asia-Pac. J. Chem. Eng.*, 2016, **11**, 60–69.

89 M. Mon, R. Bruno, E. Tiburcio, A. Grau-Atienza, A. Sepúlveda-Escribano, E. V. Ramos-Fernandez, A. Fuoco, E. Esposito, M. Monteleone, J. C. Jansen, J. Cano, J. Ferrando-Soria, D. Armentano and E. Pardo, *Chem. Mater.*, 2019, **31**, 5856–5866.

90 Y. Zhou, Y. Wang, Y. Song, S. Zhao, M. Zhang, G. Li, Q. Guo, Z. Tong, Z. Li, S. Jin, H.-B. Yao, M. Zhu and T. Zhuang, *Nat. Commun.*, 2024, **15**, 251.

91 C. Li, H. Schopmans, L. Langer, S. Marschner, A. Chandresh, J. Buerck, Y. Tsuchiya, A. Chihaya, W. Wenzel, S. Braese, M. Kozlowska and L. Heinke, *Angew. Chem., Int. Ed.*, 2023, **62**, e202217377.

92 R. Zhai, Y. Xiao, Z. Gu and J. Zhang, *Nano Res.*, 2022, **15**, 1102–1108.

93 X.-X. Yang, C. Li, S.-M. Chen, Z.-G. Gu and J. Zhang, *Chem. – Eur. J.*, 2024, **30**, e202400350.

94 C. Li, X.-X. Yang, M.-Y. Zheng, Z.-G. Gu and J. Zhang, *Adv. Funct. Mater.*, 2024, **34**, 2401102.